Cell Stem Cell

Short Article

Declining lamin B1 expression mediates age-dependent decreases of hippocampal stem cell activity

Graphical abstract

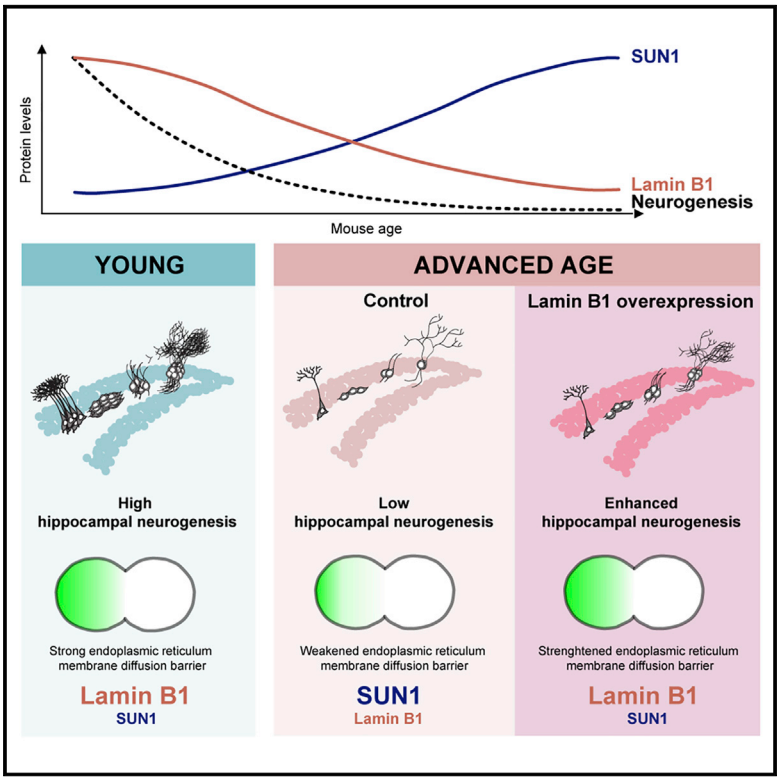

Highlights

- Lamin B1 is downregulated with age in neural stem cells (NSCs)
- SUN1 protein levels increase in aged NSCs
- Lamin B1 and SUN1 modulate ER membrane barrier strength
- Balancing lamin B1 expression enhances neurogenesis in the aged hippocampus

Authors

Muhammad Khadeesh bin Imtiaz, Baptiste N. Jaeger, Sara Bottes, Raquel A.C. Machado, Mojca Vidmar, Darcie L. Moore, Sebastian Jessberger

Correspondence

darcie.moore@wisc.edu (D.L.M.), jessberger@hifo.uzh.ch (S.J.)

In Brief

Advancing age impairs neural stem cell (NSC) function and causes a drop in the number of newly generated hippocampal neurons. bin Imtiaz et al. reveal a lamin-B1-mediated, cell-intrinsic mechanism that regulates hippocampal progenitor aging and show that restoring lamin B1 levels in the aged mouse hippocampus enhances stem cell proliferation and neurogenesis.

bin Imtiaz et al., 2021, Cell Stem Cell *28*, 1–11
May 6, 2021
https://doi.org/10.1016/j.stem.2021.01.015

CellPress

Cell Stem Cell

CellPress

Short Article

Declining lamin B1 expression mediates age-dependent decreases of hippocampal stem cell activity

Muhammad Khadeesh bin Imtiaz,[1] Baptiste N. Jaeger,[1] Sara Bottes,[1] Raquel A.C. Machado,[1] Mojca Vidmar,[1] Darcie L. Moore,[2,*] and Sebastian Jessberger[1,3,*]

[1]Laboratory of Neural Plasticity, Faculties of Medicine and Science, Brain Research Institute, University of Zurich, 8057 Zurich, Switzerland

[2]Department of Neuroscience, University of Wisconsin-Madison, Madison, WI 53705, USA

[3]Lead contact

*Correspondence: darcie.moore@wisc.edu (D.L.M.), jessberger@hifo.uzh.ch (S.J.)

https://doi.org/10.1016/j.stem.2021.01.015

SUMMARY

Neural stem cells (NSCs) generate neurons throughout life in the hippocampal dentate gyrus. With advancing age, levels of neurogenesis sharply drop, which has been associated with a decline in hippocampal memory function. However, cell-intrinsic mechanisms mediating age-related changes in NSC activity remain largely unknown. Here, we show that the nuclear lamina protein lamin B1 (LB1) is downregulated with age in mouse hippocampal NSCs, whereas protein levels of SUN-domain containing protein 1 (SUN1), previously implicated in Hutchinson-Gilford progeria syndrome (HGPS), increase. Balancing the levels of LB1 and SUN1 in aged NSCs restores the strength of the endoplasmic reticulum diffusion barrier that is associated with segregation of aging factors in proliferating NSCs. Virus-based restoration of LB1 expression in aged NSCs enhances stem cell activity *in vitro* and increases progenitor cell proliferation and neurogenesis *in vivo*. Thus, we here identify a mechanism that mediates age-related decline of neurogenesis in the mammalian hippocampus.

INTRODUCTION

Advancing age is associated with a decline in somatic stem cell numbers and/or function (Ermolaeva et al., 2018). Similar to other organs, the proliferative activity of stem cells is reduced with age in the mammalian brain, where neural stem cells (NSCs) generate new neurons throughout life in two main neurogenic regions: the subventricular zone (SVZ) lining the lateral ventricles and the hippocampal dentate gyrus (DG) (Gonçalves et al., 2016; Obernier and Alvarez-Buylla, 2019). Within the DG, new neurons have been implicated in hippocampal-dependent cognition and mood control (Anacker and Hen, 2017; Gonçalves et al., 2016). The age-related decline of neurogenesis has been associated with memory impairment (Drapeau et al., 2003; Katsimpardi and Lledo, 2018). Furthermore, perturbations that enhance neurogenesis, ranging from voluntary physical activity and environmental enrichment to parabiosis, efficiently ameliorate cognitive impairment and improve memory function in aged mice (Kempermann et al., 2002; van Praag et al., 2005; Villeda et al., 2011). Over the last decade, a number of niche-derived molecular factors have been identified that mediate age-related loss of neurogenesis (Kalamakis et al., 2019; Katsimpardi et al., 2014; Kempermann, 2015; Meng et al., 2018; Seib et al., 2013; Silva-Vargas et al., 2016). Despite recent advances (Beckervordersandforth et al., 2017; Kalamakis et al., 2019; Leeman et al., 2018; Morrow et al., 2020), cell-intrinsic mechanisms that are affected by advancing age in NSCs remain poorly understood.

Lamins, intermediate filaments of the nuclear lamina that, among other functions, anchor chromatin at the nuclear periphery, have been previously implicated as cell-intrinsic mediators of cellular aging and senescence (de Leeuw et al., 2018; Scaffidi and Misteli, 2008; Shimi et al., 2011). The lamin protein family is composed of lamin A and C (LA and LC; A-type) and lamin B1 and B2 (LB1 and LB2; B-type). Most prominently, it has been found that mutations in LA, encoded by *LMNA*, are causally linked to Hutchinson-Gilford progeria syndrome (HGPS), a disease of premature aging, by disrupting nuclear shape and function (Goldman et al., 2004; Larrieu et al., 2014). These *LMNA* mutations result in the expression of a truncated LA, called progerin, that subsequently leads to increased levels of the nuclear envelope protein SUN-domain containing protein 1 (SUN1), a component of the linker of nucleoskeleton and cytoskeleton (LINC) complex (Starr and Fridolfsson, 2010). Indeed, SUN1 protein upregulation appears to be a critical mediator of the detrimental effects of *LMNA* mutations on cellular function (Chen et al., 2012; Starr, 2012). Thus, alterations in nuclear lamins have been linked to cellular aging.

Interestingly, ectopic expression of progerin in hippocampal NSCs disrupts the function of a diffusion barrier in the membrane

Please cite this article in press as: bin Imtiaz et al., Declining lamin B1 expression mediates age-dependent decreases of hippocampal stem cell activity, Cell Stem Cell (2021), https://doi.org/10.1016/j.stem.2021.01.015

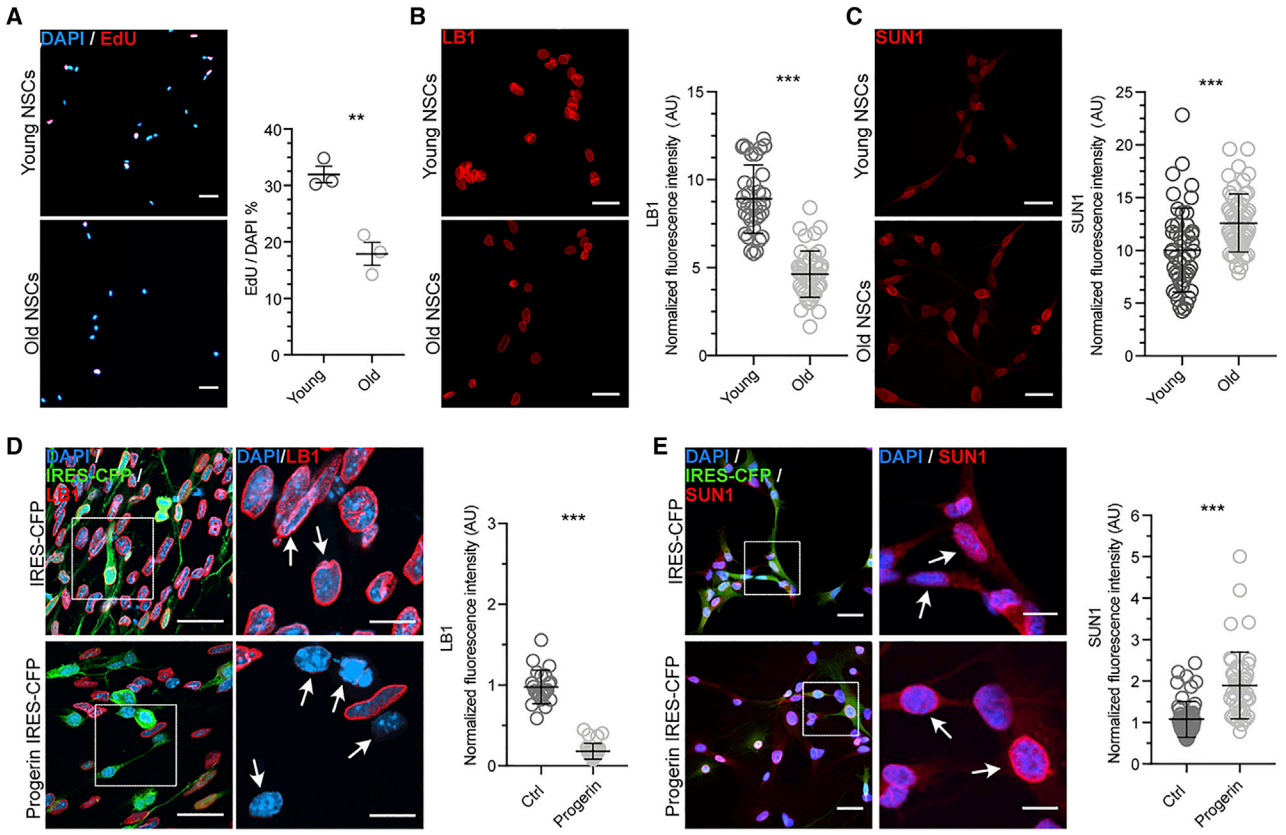

Figure 1. Age-related regulation of LB1 and SUN1 in hippocampal NSCs

(A) Proliferation of NSCs decreases with age. Shown are proliferating hippocampal NSCs derived from 6-week- (young) and 9-month-old (old) mice visualized by the incorporation of EdU (red). DAPI (blue) stains the nuclei. The percentage of EdU-positive NSCs decreases with age (n = 3; mean ± SEM; unpaired t test).

(B) Expression of LB1 decreases in old NSCs. Young and old NSCs were stained against LB1 (red). Each dot represents the fluorescent intensity of an individual cell analyzed from >3 mice (young: n = 35, old: n = 48; mean ± SD; unpaired t test).

(C) Expression of SUN1 increases in old NSCs. Young (n = 47) and old (n = 57) NSCs stained against SUN1 (red) are shown. Each dot represents the fluorescent intensity of an individual cell analyzed from >3 mice (mean ± SD; unpaired t test).

(D) Progerin overexpression reduces LB1 expression in young NSCs. Young NSCs retrovirally transduced with IRES-CFP (Ctrl) or with progerin-IRES-CFP-expressing retrovirus were stained against LB1 (red), CFP (green), and DAPI (blue). Arrows point toward progerin-transduced cells with low LB1 protein levels. Boxed regions are magnified in right panels. Each dot represents the fluorescent intensity of an individual cell (Ctrl: n = 23; progerin: n = 29; mean ± SD; unpaired t test).

(E) Progerin overexpression increases SUN1 expression in young NSCs. Young NSCs retrovirally transduced with IRES-CFP (Ctrl) or with progerin-IRES-CFP were stained against SUN1 (red), CFP (green), and DAPI (blue). Arrows point toward progerin-transduced cells with high SUN1 levels. Boxed regions are magnified in right panels. Each dot represents the fluorescent intensity of an individual cell (Ctrl: n = 55; progerin: n = 48; mean ± SD; unpaired t test).

Scale bars represent 50 μm (A), 25 μm (B–E), and 10 μm (boxed D and E); **p < 0.01; ***p < 0.001. See also Figure S1.

of the endoplasmic reticulum (ER), causing a failure to properly segregate aging factors (Moore et al., 2015). The ER diffusion barrier is a conserved mechanism between budding yeast, *C. elegans*, and mammalian cells, specifically NSCs, mediating asymmetric segregation of aging factors, such as damaged proteins and extrachromosomal DNA, during cell divisions (Lee et al., 2016; Moore et al., 2015; Shcheprova et al., 2008). Notably, not only ectopic expression of progerin, used previously to induce cellular aging, weakens the barrier, but also advancing age of NSCs is associated with reduced barrier strength (Miller et al., 2013; Moore et al., 2015). These findings suggest that lamins, which along with other components of the nuclear envelope integrate into the ER membrane during mammalian cell divisions, may be involved in regulating ER diffusion barrier strength and cell division (Moir et al., 2000; Rabut et al., 2004). Together with previous data showing that LB1 is highly expressed in hippocampal NSCs, we hypothesized that alterations in LB1 levels may contribute to cell-intrinsic, age-dependent changes in hippocampal progenitor cell activity (Bracko et al., 2012; Toda et al., 2017).

We show here that LB1 protein levels are decreased in aged progenitors *in vitro* and *in vivo* together with a concomitant increase in SUN1 protein levels. Further, LB1 and SUN1 regulate ER diffusion barrier strength, and recovering LB1 expression is sufficient to rescue proliferation deficits in aged NSCs. Finally, we probe the relevance of LB1 for the decline of progenitor

Please cite this article in press as: bin Imtiaz et al., Declining lamin B1 expression mediates age-dependent decreases of hippocampal stem cell activity, Cell Stem Cell (2021), https://doi.org/10.1016/j.stem.2021.01.015

CellPress

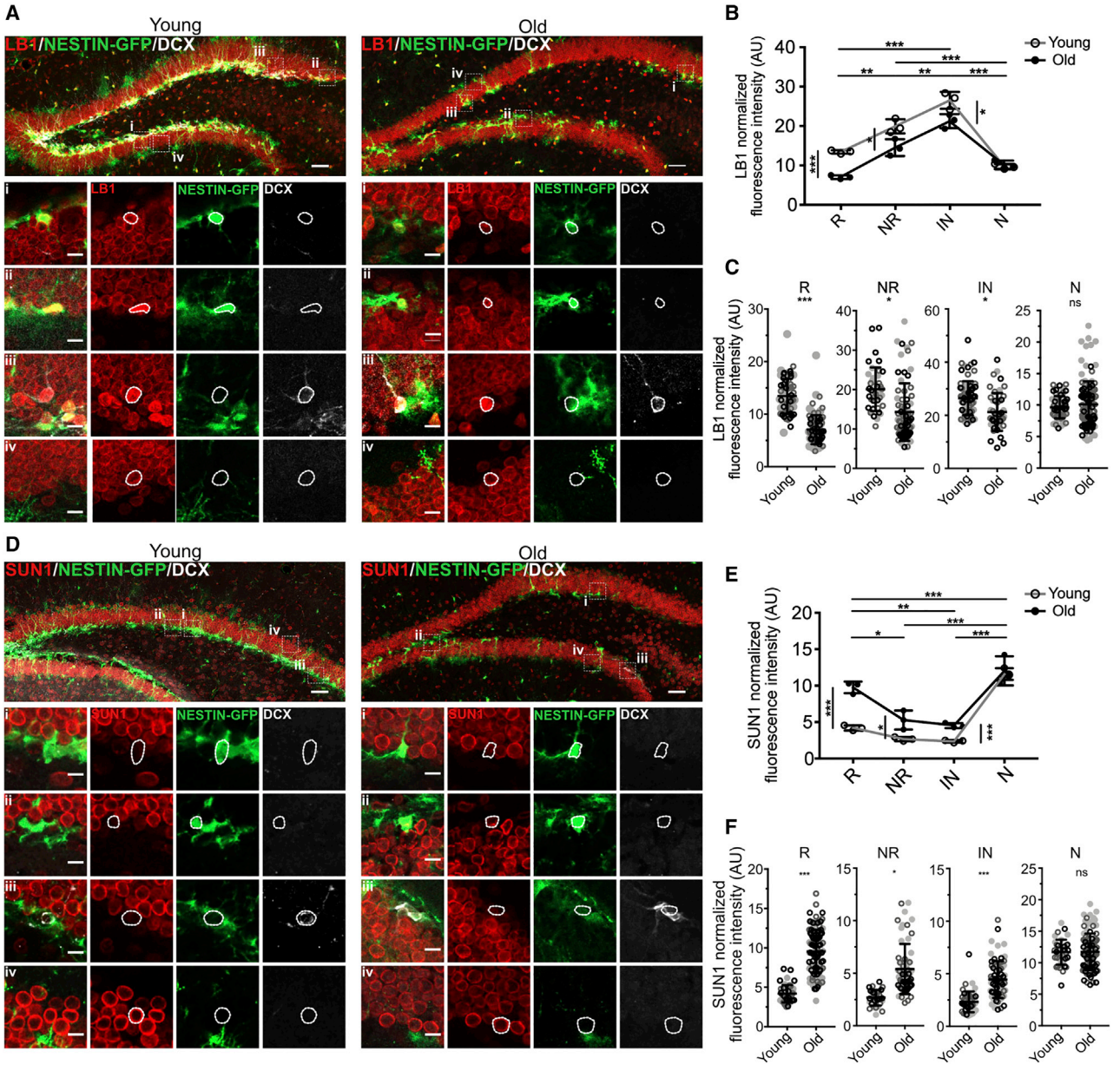

Figure 2. SUN1 and LB1 are differentially regulated with age in the mouse hippocampus

(A) Representative images of young (left) and old (right) hippocampi stained against LB1 (red), DCX (white), and nestin-GFP (green). (i) Cells with nestin-GFP and a radial process were identified as radial glia cells (R) cells and are enlarged below each image. (ii) Cells with nestin-GFP but without a radial process were identified as non-radial glia cells (NR) cells. (iii) Cells positive for DCX were identified as immature neurons (INs). (iv) Cells in the molecular layer were identified as neurons (Ns).

(B) Quantified fluorescent intensities for LB1 normalized to the background illustrating the differential regulation of SUN1 in the four cell types are shown. Each dot represents the average of a single animal for each cell type (n = 3; mean ± SD; p values shown for one-way ANOVA test for young animals between cell types and unpaired t test between old and young).

(C) Quantified fluorescent intensities for LB1 normalized to background are compared between old and young animals for each cell type. Each dot represents a cell with the three animals being represented by a filled circle, a black outline, or a gray outline (total number of cells analyzed: R: n = 63 [young] and 86 [old], NR: n = 42 [young] and 75 [old], IN: n = 75 [young] and 47 [old], N: n = 62 [young] and 123 [old]; mean ± SD; t test performed with n = 3 corresponding to the number of animals for each cell type).

(D) Representative images of young (left) and old (right) hippocampi stained against SUN1 (red), DCX (white), and nestin-GFP (green). (i) Cells with nestin-GFP and a radial process were identified as R cells and are enlarged below each image. (ii) Cells with nestin-GFP but without a radial process were identified as NR cells. (iii) Cells positive for DCX were identified as INs. (iv) Cells in the molecular layer were identified as Ns.

(E) Quantified fluorescent intensities for SUN1 normalized to the background illustrating the differential regulation of SUN1 in the four cell types. Each dot represents the average of a single animal for each cell type (n = 3; mean ± SD; p values shown for one-way ANOVA test for young animals between cell types and unpaired t test between old and young).

(legend continued on next page)

Please cite this article in press as: bin Imtiaz et al., Declining lamin B1 expression mediates age-dependent decreases of hippocampal stem cell activity, Cell Stem Cell (2021), https://doi.org/10.1016/j.stem.2021.01.015

proliferation within the aged hippocampus and show that overexpression of LB1 selectively in the neurogenic lineage is sufficient to enhance neurogenesis *in vivo*.

RESULTS

Age-dependent regulation of LB1 and SUN1 in hippocampal NSCs

Based on previous gene expression analyses showing high expression of LB1 in hippocampal NSCs and the finding that overexpression of the *LMNA* mutant progerin affects NSC behavior, we analyzed LB1 and SUN1 expression in NSCs isolated from the DG of 6 weeks (young adult) and 9-month-old mice (given that the drop of neurogenesis occurs between 2 and 8 months of age, we hereafter refer to 9-month-old mice as "aged/old" in the context of NSC function; Ben Abdallah et al., 2010; Moore et al., 2015; Toda et al., 2017). As described previously (Moore et al., 2015), NSCs isolated from the aged DG show a decrease in cell proliferation as measured by 5-Ethynyl-2′-deoxyuridine (EdU) pulse labeling when grown in conventional adherent monolayer cultures for up to 60 days *in vitro* (DIV) (Figures 1A and S1A). Because proliferation of aged NSCs returns to levels similar to young NSCs >60 DIV, all experiments analyzing aged NSCs were performed with cells <60 DIV (Figure S1B). Associated with the age-related reduction in proliferation, we found a decrease in LB1 protein levels in aged NSCs although SUN1 protein levels were increased (Figures 1B and 1C). In contrast to LB1, we found Lamin B2 protein, a B-type lamin related to LB1, increased although LA/LC levels were unchanged in aged NSCs (Figures S1C and S1D). Supporting age-related dynamic regulation of LB1 and SUN1, we found that ectopic expression of progerin in young NSCs was sufficient to reduce protein levels of LB1 while upregulating SUN1 levels (Figures 1D and 1E). Progerin expression has been previously described as a model of induced aging, even though progerin is not expressed in the central nervous system in HGPS patients due to a non-coding RNA-mediated decay (Jung et al., 2012; Miller et al., 2013).

We next analyzed the regulation of LB1 and SUN1 with age in the endogenous hippocampal niche. Similar to previous reports, we found expression of LB1 in nestin-GFP-labeled radial glia-like (R) and non-radial glia-like (NR) progenitors (Figures 2A and 2B; Takamori et al., 2007). In addition, LB1 was highly expressed in doublecortin (DCX)-expressing newborn neurons, suggesting a function for LB1 not only in stem cells but also for their neuronal progeny (Figures 2A and 2B; Mahajani et al., 2017; Takamori et al., 2007). We found that LB1 was downregulated in 12-month-old mice compared to 2-month-old young adult mice in nestin-GFP-labeled R, NR cells as well as in immature neurons (INs) (Figure 2C), indicating that LB1 levels are reduced within the neurogenic lineage of the aging hippocampus. LB1 levels were not affected with age in more mature neurons (Ns) (Figures 2B and 2C). In young mice, we found that SUN1 is expressed in R and to a lesser extent in NR cells and DCX-labeled INs before it becomes upregulated in mature granule cells (Ns; Figures 2D and 2E). Corroborating the *in vitro* results, protein levels of SUN1 substantially increased in aged R cells and NR cells as well as in immature neurons although levels in mature neurons were not affected by advancing age (Figures 2E and 2F). Outside of the subgranular zone, we observed no changes in LB1 and SUN1 protein levels with age in glial fibrillary acidic protein (GFAP)-labeled hilar astrocytes but found that LB1 protein was upregulated with age in SOX10-expressing cells of the oligodendrocytic lineage although SUN1 was unchanged (Figures S2A–S2D). Interestingly, the age-associated regulation of LB1 and SUN1 in R cells occurred already in 5-month-old mice when levels of neurogenesis have already sharply dropped (Figures S2E and S2F; Ben Abdallah et al., 2010; Bracko et al., 2012; Moore et al., 2015; Toda et al., 2017). Together, these findings identify LB1 and SUN1 to be dynamically regulated with age in the hippocampal neurogenic lineage.

LB1 and SUN1 affect ER membrane barrier strength

Given that progerin was sufficient to downregulate levels of LB1 and at the same time increase SUN1 protein, we next asked whether LB1 and SUN1 regulate each other's protein levels. Indeed, we observed that viral overexpression of LB1 in aged NSCs efficiently decreased levels of SUN1 (Figures S3A and S3B). In contrast, SUN1 knockdown using virally expressed short hairpin RNA (shRNA) directed against the coding mRNA for SUN1 in aged NSCs did not change LB1 protein levels (data not shown). These findings suggest that regulation of LB1 and SUN1 is unidirectionally connected in hippocampal NSCs, indicating that a previously described functional link between lamins and components of the LINC complex is also present in NSCs (Haque et al., 2006). We next analyzed the consequences of differential expression of LB1 and SUN1 on NSC function. We had previously described the establishment of a diffusion barrier in the membrane of the endoplasmic reticulum (ER) that may contribute to the segregation of aging factors in proliferative NSCs (Moore et al., 2015). In analogy to the ER membrane diffusion barrier in budding yeast and *C. elegans*, we found that the strength of the barrier in NSCs is regulated with age and is functionally associated with the asymmetric segregation of aging factors (Lee et al., 2016; Moore et al., 2015; Shcheprova et al., 2008). Using fluorescence loss in photobleaching (FLIP) experiments of green fluorescent protein (GFP) tagged to the ER membrane (using Sel1L-based targeting; hereafter called ER membrane) or ER lumen (using KDEL targeting; hereafter called ER lumen), we tested whether differential expression of LB1 and SUN1 correlate with the strength of the ER barrier (Figures 3A and S3C–S3F; Video S1). Corroborating previous results obtained using GFP-tagged Sec61, an ER membrane protein, we found that aged NSCs have a weakened ER barrier compared to young adult NSCs (Figures 3B and 3C; Video S1; Moore et al., 2015). Virus-based restoration of LB1 expression in aged NSCs rescued barrier strength (Figures 3D and 3E; Video S2). Supporting functional connectivity between lamin/LINC

(F) Quantified fluorescent intensities for SUN1 normalized to background are compared between old and young animals for each cell type. Each dot represents a cell with the three animals being represented by a filled circle or a black or gray outline (total number of cells analyzed: R: n = 44 [young] and 116 [old], NR: n = 31 [young] and 61 [old], IN: n = 53 [young] and 74 [old], N: n = 39 [young] and 98 [old]; t test performed with n = 3 corresponding to the number of animals for each cell type).

Scale bars represent 50 μm (A and D) and 10 μm (A and D insets). $p > 0.05$ (ns); *$p < 0.05$; **$p < 0.01$; ***$p < 0.001$. See also Figure S2.

Please cite this article in press as: bin Imtiaz et al., Declining lamin B1 expression mediates age-dependent decreases of hippocampal stem cell activity, Cell Stem Cell (2021), https://doi.org/10.1016/j.stem.2021.01.015

CellPress

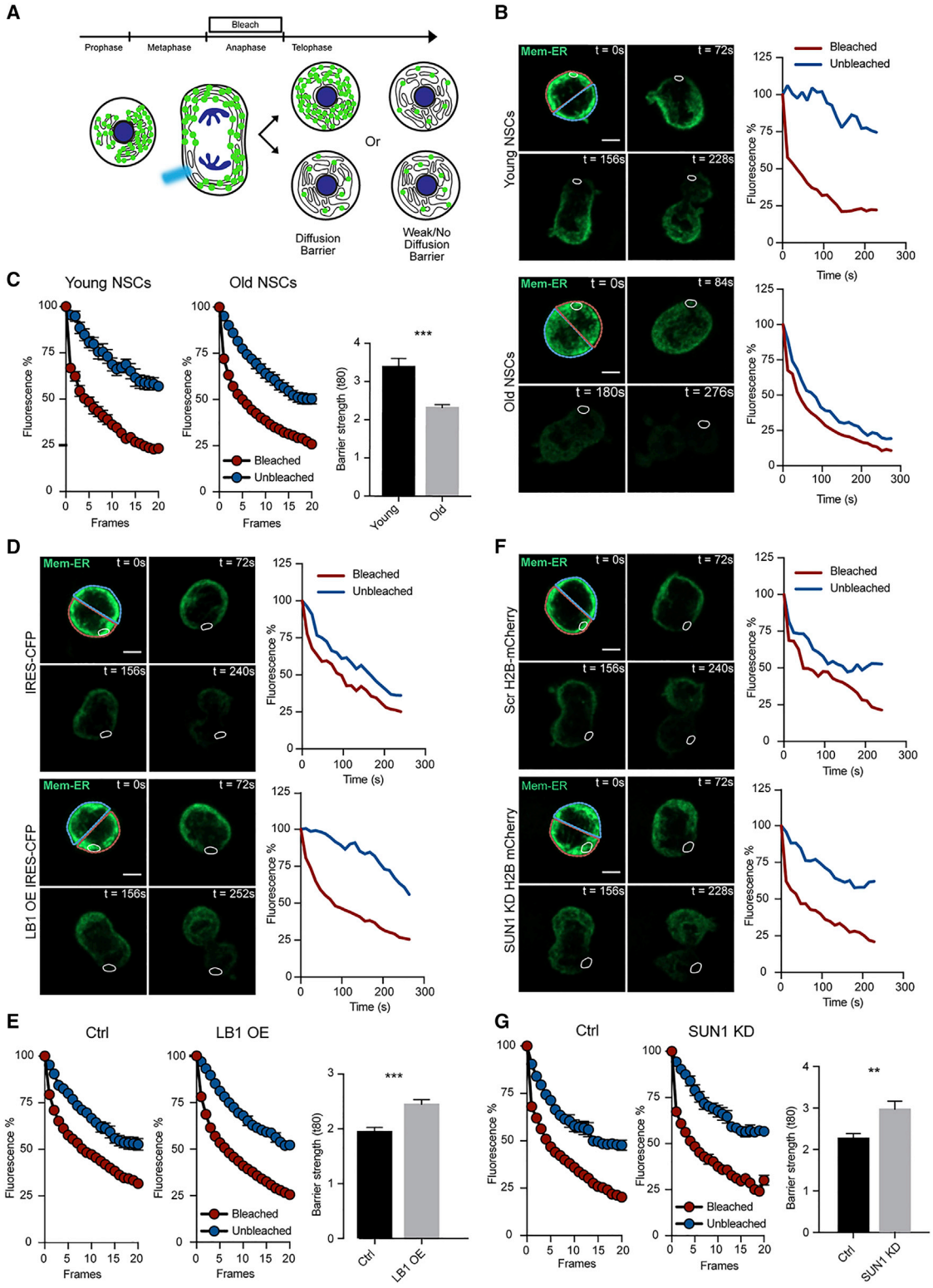

Figure 3. LB1 overexpression and SUN1 knockdown rescue the barrier strength in aged NSCs

(A) A schematic of the fluorescence loss in photobleaching (FLIP) experiment is shown. An endoplasmic reticulum (ER) membrane protein tagged with GFP is overexpressed. Once the cell enters anaphase, an area close to the dividing plane is bleached continuously until the cell completes cytokinesis. If there were a barrier to diffusion between the two compartments of the dividing cell, only the bleached compartment would lose fluorescence (diffusion barrier). In contrast, the absence of or a weak ER-membrane diffusion barrier results in loss of fluorescence in the bleached and unbleached compartments (weak/no diffusion barrier).

(legend continued on next page)

Please cite this article in press as: bin Imtiaz et al., Declining lamin B1 expression mediates age-dependent decreases of hippocampal stem cell activity, Cell Stem Cell (2021), https://doi.org/10.1016/j.stem.2021.01.015

complexes in regulating the ER diffusion barrier, we similarly found that shRNA-mediated downregulation of aging-induced SUN1 was sufficient to restore barrier strength (Figures 3F, 3G, and S3G; Video S2). In contrast, deletion of LB1 or overexpression of SUN1 in young NSCs did not affect ER barrier strength (Figures S3H–S3M; Video S3). Together, these findings demonstrate that increasing (LB1) or decreasing (SUN1) age-related changes in protein levels of LB1 and SUN1 are sufficient to rescue the weakening of the ER diffusion barrier that occurs with age.

LB1 expression in aged progenitor cells enhances cell proliferation and neurogenesis *in vivo*

After showing that LB1 is downregulated with age and that re-expression of LB1 rescues barrier strength in dividing NSCs, we next tested whether LB1 is sufficient to increase NSC proliferation in aged NSCs. Indeed, we found that virus-based overexpression of LB1 in aged NSCs increased levels of proliferation in aged NSCs, as measured by EdU pulse labeling and cell-cycle analyses (Figures 4A, S4A, and S4B). SUN1 overexpression in young NSCs, mimicking the situation in aged cells (Figure 1C), did not affect proliferation (Figure S4C). Given that LB1 has higher expression levels in proliferating versus quiescent young NSCs (Figure S4D; Knobloch et al., 2017), we tested the function of LB1 in quiescence entry and found that LB1 overexpression reduced entry into quiescence when young cells were exposed to bone morphogenetic protein 4 (BMP4), a model of NSC quiescence (Figure 4B; Martynoga et al., 2013; Mira et al., 2010), suggesting a role for LB1 in the cell cycle as described before (Tsai et al., 2006). We next analyzed whether LB1 overexpression affects the gene expression profiles of young versus aged NSCs. Similar to previous data (Moore et al., 2015), we found robust differences between young and aged NSCs, although aged cells overexpressing LB1 remained similar to aged control cells and only led to mild changes in gene expression (Figures S4E–S4H; Table S1).

Probing a potential role for hippocampal neurogenesis *in vivo*, we made use of a tissue-specific approach to selectively enhance expression of LB1 in adult NSCs and their progeny: we designed Cre-dependent lentiviral expression constructs of LB1 (flanked by cyan fluorescent protein [CFP] expression cassette; hereafter called floxed-LB1-CFP) that were injected into 6-month-old mice expressing tamoxifen (Tam)-inducible Cre recombinase from the regulatory elements of the GLI family zinc finger 1 (Gli1) promoter, active in hippocampal R cells, crossed with a tdTomato reporter mouse line (hereafter called Gli1/tdTomato; Figure 4C; Ahn and Joyner, 2005; Bottes et al., 2021). Thus, Gli1-expressing NSCs that were transduced with virus will express tdTomato and LB1-CFP upon treatment with Tam, causing labeling with yellow fluorescence. We used 6- to 7-month-old mice given that neurogenesis is already substantially decreased at this age and because we found LB1 protein levels to be reduced at this age (Figures S2E and S2F; Ben Abdallah et al., 2010). 2 days after stereotactic injections of floxed-LB1-CFP lentiviruses or respective control viruses (floxed-CFP) into the hippocampus, we injected Gli1/tdTomato mice with three doses of Tam, allowing for Cre-based activation of LB1 expression in R cells and their daughter cells (Figures 4C–4E). Given the chosen targeting strategy, we first compared numbers of yellow cells (i.e., tdTomato- and CFP-labeled cells, detected with an antibody against GFP) in Gli1/tdTomato mice 14 days after the last Tam injection and confirmed virus-based overexpression of LB1 in recombined cells (Figures 4D and 4E). We found that re-expression of LB1 led to enhanced proliferation in targeted (yellow) neurogenic cells (Figure 4F). Within the pool of proliferative cells, the relative ratio of dividing R and NR was maintained between LB1-overexpressing and control cells (Ctrl: R: 3.5%, NR: 96.5% ± 3.5%, mean ± SEM; LB1 OE: R: 5.4%, NR: 94.6% ± 1.6% mean ± SEM; $p = 0.46$, paired t test). We next tested whether LB1 overexpression also enhances the generation of new neurons in mice of advancing age. 4 weeks after Tam injections, we found an increase of newborn neurons, identified by the expression of yellow fluorescence (being derived from Gli1/tdTomato cells targeted with floxed-LB1-CFP or control viruses; Figure 4G). In analogy to aged NSCs *in vitro* (Figure S3B), we found that levels of SUN1 were decreased in LB1-overexpressing (yellow) R cells (Figure 4H). Further, LB1 overexpression affected levels of mono- and poly-ubiquitinated proteins (Ub) within the neurogenic lineage, as we observed elevated levels of Ub in NR cells compared to R cells after overexpression of LB1 *in vivo* (Figure S4I), suggesting that LB1 overexpression may enhance asymmetric segregation of Ub, as described previously (Moore et al., 2015). Thus, targeting LB1 in the aged hippocampus is sufficient to enhance Gli1-targeted stem cell proliferation and neurogenesis, demonstrating functional significance of the age-related

(B) Time course of a FLIP experiment performed in a young and old NSC overexpressing ER-membrane protein tagged with sfGFP (MemER-GFP) is shown. A selected area is bleached continuously (white). The fluorescence in the bleached compartment (red) and the unbleached compartment (blue) was measured. Traces of the fluorescence for the bleached and the unbleached compartments of each cell over time are shown (right).
(C) The strength of the barrier decreases in old NSCs. Quantification of fluorescence intensities in bleached and unbleached compartment for young and old NSCs is shown (left; young: n = 9, old: n = 19; mean ± SEM). Quantification of barrier strength at t = 80 s for young and old NSCs is shown (right; mean ± SEM).
(D) LB1 overexpression (OE) in old NSCs rescues the barrier strength. Old NSCs expressing the ER-membrane marker (MemER-GFP) were transduced with control (IRES-CFP) or with LB1-overexpressing retrovirus (LB1-IRES-CFP). Time-lapse of a FLIP experiment performed on a control (top) and a LB1-overexpressing (bottom) cell is shown. Traces of the fluorescence for the bleached and the unbleached compartments for both cells over time are shown (right).
(E) The rescue of the barrier strength by LB1 OE is illustrated here. Averages of the fluorescence intensities of bleached and unbleached compartment for control and LB1-overexpressing cells is shown (left; Ctrl: n = 15, LB1 OE: n = 16; mean ± SEM). Quantification of the barrier strength at t = 80 s for control and LB1-overexpressing cells is shown (right; mean ± SEM; unpaired t test).
(F) SUN1 knockdown (KD) in old NSCs rescues the barrier strength. Old NSCs expressing the ER-membrane marker (MemER-GFP) were transduced with a retrovirus expressing either a scrambled shRNA (Scr H2B-mCherry) or an shRNA targeting SUN1 (SUN1 KD H2B-mCherry). Time-lapse of a FLIP experiment performed on a control (top) and a SUN1 knockdown (bottom) cell is shown. Traces of the fluorescence for the bleached and the unbleached compartments are shown.
(G) Rescue of the barrier strength by SUN1 KD. Averages of the fluorescence intensities of bleached and unbleached compartment for control and SUN1 knockdown cells are shown (left; Ctrl: n = 10, SUN1 KD: n = 10; mean ± SEM). Quantification of the barrier strength at t = 80 s for control and LB1-overexpressing cells is shown (right; mean ± SEM; unpaired t test).
Scale bars represent 5 μm (B, D, and F). $^{**}p < 0.01$; $^{***}p < 0.001$. See also Figure S3.

Please cite this article in press as: bin Imtiaz et al., Declining lamin B1 expression mediates age-dependent decreases of hippocampal stem cell activity, Cell Stem Cell (2021), https://doi.org/10.1016/j.stem.2021.01.015

CellPress

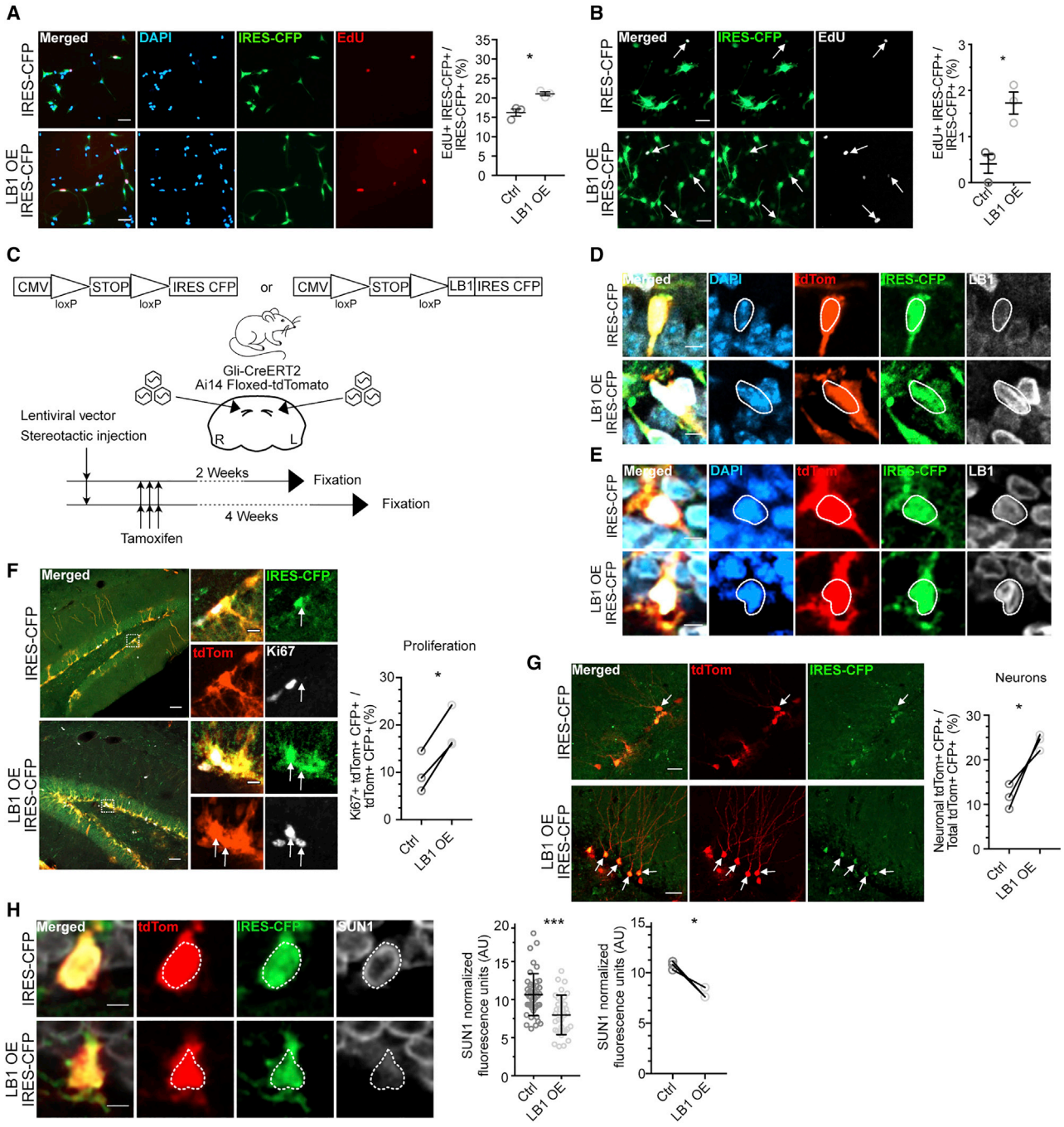

Figure 4. Targeted LB1 overexpression enhances progenitor proliferation and neurogenesis in the aged hippocampus

(A) LB1 overexpression increases proliferation of old NSCs. Cells transduced with the control (IRES-CFP) or with LB1-overexpressing retrovirus were EdU pulsed for 1 h before they were stained against IRES-CFP (green), DAPI (blue), and EdU (red). IRES-CFP+ and EdU+ cells were counted and then divided by the total number of IRES-CFP+ cells (n = 3 experiments; mean ± SEM; unpaired t test).

(B) LB1 overexpression decreases quiescence. Quiescence was induced using BMP4 in young NSCs that were electroporated with control (IRES-CFP) or LB1-overpressing plasmid. 2 days after induction of quiescence, NSCs were pulsed with EdU for 1 h before they were stained against IRES-CFP (green), DAPI (blue), and EdU (white). IRES-CFP+ and EdU+ cells were counted and then divided by the total number of IRES-CFP+ cells (n = 3 experiments; mean ± SD; unpaired t test).

(C) Schematic of the experimental outline. Floxed control (IRES-CFP) and floxed LB1-overexpressing (LB1-IRES-CFP) lentiviruses were stereotactically injected into the DG of 6- to 7-month-old, Gli-CreER^{T2}/Ai14 floxed-tdTomato mice. LB1-overexpressing virus was injected in the left side, and the control was injected in the right side (n = 6). 2 days after the injection, the mice were injected with Tam over 3 days to induce recombination of the tdTomato reporter and allowing for lentiviral transgene expression. One cohort was perfused 2 weeks (n = 3) although the other cohort was perfused after 4 weeks (n = 3). Recombined cells express tdTomato with a subset also being positive for lentivirally expressed IRES-CFP, resulting in yellow fluorescence.

(legend continued on next page)

Please cite this article in press as: bin Imtiaz et al., Declining lamin B1 expression mediates age-dependent decreases of hippocampal stem cell activity, Cell Stem Cell (2021), https://doi.org/10.1016/j.stem.2021.01.015

downregulation of LB1 protein in hippocampal progenitors *in vivo*.

DISCUSSION

Here, we show that components of the lamin-LINC complex, LB1 and SUN1, are dynamically regulated with age in hippocampal NSCs. Although levels of LB1 protein drop in parallel to reduced proliferation of adult NSCs, SUN1 protein increases with advancing age. Normalizing LB1 and SUN1 levels in old NSCs rescues the strength of an ER diffusion barrier that mediates asymmetric segregation of aging factors in proliferating NSCs. Moreover, restoring decreased levels of LB1 is sufficient to enhance proliferation of progenitors and neurogenesis within the hippocampal niche in mice of advanced age. Thus, we here identify a novel mechanism of how age-mediated, cell-intrinsic molecular alterations affect stem cell behavior in the adult mammalian brain.

Lamins have been previously implicated in aging and NSC biology (de Leeuw et al., 2018; Shimi et al., 2011). Although mutations in LA/LC do not lead to neurological phenotypes (due to low expression of A-type lamins in the central nervous system), it has been shown that B-type lamins are critically involved in the development of the brain (Coffinier et al., 2011; Mahajani et al., 2017). However, LB1 or LB2 have not been associated with aging in the context of NSCs. How could a decrease in LB1 mediate age-related changes in NSC behavior? It previously has been shown that LA directly interacts with SUN1, a component of the LINC complex that is localized to the inner nuclear membrane. The nucleoplasmic domain of SUN1 interacts with lamins, and its luminal domain binds the KASH domains of nesprins present in the outer nuclear membrane (Haque et al., 2006; Tapley and Starr, 2013). Mutations in *LMNA* lead to accumulation of SUN1 in mouse models and fibroblasts derived from HGPS patients, which has been attributed to enhanced stability of SUN1 under these conditions (Chen et al., 2012). Thus, SUN1 protein may be stabilized and therefore accumulate with aging, similar to what has been described for HGPS-associated changes in the LINC complex (Mattioli et al., 2011; Starr, 2012). In line with this, we found that LB1 overexpression in aged NSCs normalized expression levels of SUN1. Whether the observed age-dependent regulation of LB1 and SUN1 occurs via direct interactions between SUN1 and LB1 proteins remains unclear. Notably, we here show that SUN1 is not only regulated in disease-associated laminopathies, such as HGPS, but that an increase in SUN1 also occurs with physiological aging in adult hippocampal progenitors. SUN1 was not regulated with age in hilar astrocytes, dentate OPCs, or mature neurons. Whether the age-related increase of SUN1 protein levels is tissue specific or can be also observed in other somatic stem cells during aging needs to be tested. Also, the increase observed in LB1 levels in aged cells of the oligodendrocytic lineage (labeled with SOX10) needs further analyses. Interestingly, the up- and downregulation for SUN1 and LB1 proteins occurred independent of changes in gene expression levels in cultured cells (Moore et al., 2015), suggesting that post-transcriptional mechanisms lead to altered expression of LB1 and SUN1 with age.

Increase of SUN1 and decrease in LB1 expression in hippocampal progenitors occurs relatively early in life (around 4–6 months of age in rodents). Importantly, changes in LB1/SUN1 expression occur simultaneously with a drop in neurogenesis by around 80% from 2 to 8 months of age (Ben Abdallah et al., 2010; Gonçalves et al., 2016; Katsimpardi and Lledo, 2018; Kuhn et al., 1996). After this time, levels of neurogenesis plateau and remain low but detectable throughout the remaining lifespan (Ben Abdallah et al., 2010; Ziebell et al., 2018). Several possibilities may explain the observed reduction in neurogenesis with altered LB1/SUN1 levels. Altered interactions of chromatin between lamin-LINC complexes may be detrimental for gene expression causing age-related changes in stem cell behavior, even though we did not observe substantial changes of gene expression upon LB1 overexpression in aged hippocampal progenitors. Interestingly, we found that LB1 overexpression reduces entry into BMP4-induced quiescence of young NSCs. Thus, restoring levels of LB1 in aged R cells may enhance quiescence exit, which has been previously suggested to be impaired in aged NSCs (Kalamakis et al., 2019; Morrow et al., 2020). However, we did not observe a relative increase of R cell proliferation in LB1-overexpressing cells compared to control cells, indicating that LB1 enhances both the proliferation of R and NR cells. Changes in lamin-LINC protein levels may cause biophysical changes in nuclear envelope functionality that could impact on cellular behavior (Schreiber and Kennedy, 2013). Our data indicate that both LB1 and SUN1 affect the strength of an ER

(D) LB1 overexpression in tdTomato+ (red) and IRES-CFP+ (green) cells in the 2-week cohort. Upper row shows control cells expressing IRES-CFP and tdTomato; lower row shows cells overexpressing LB1 (white) that are IRES-CFP+/tdTomato+. Note the overexpression of LB1 in yellow cells.
(E) LB1 overexpression in tdTomato+ (red) and IRES-CFP+ (green) cells in the 4-week cohort. Upper row shows control cells expressing IRES-CFP and tdTomato; lower row shows cells overexpressing LB1 (white) that are IRES-CFP+ and tdTomato+. Note the overexpression of LB1 in yellow cells.
(F) LB1 overexpression increases proliferation of hippocampal progenitors in old mice. Representative images of the DG transduced with the control virus (top) and LB1-overexpressing virus (bottom) are shown. Boxed areas are enlarged. The number of tdTomato+ (red), IRES-CFP+ (green), and Ki67+ (white) cells were counted for both conditions. The percentage of triple-positive (Ki67+ tdTomato+ IRES-CFP+) cells over double positive (tdTomato+ IRES-CFP+) was calculated and plotted (right). Each point represents a DG and is connected to the contralateral results with a line (Ctrl: n = 3, LB1 OE n = 3; paired t test).
(G) LB1 overexpression increases the number of newly generated neurons in old mice. Representative images of the DG transduced with the control virus (top) and LB1-overexpressing virus (bottom) are shown. Cells with neuronal morphology and positive for tdTomato (red) and IRES-CFP (green) were counted for both conditions (arrows). The percentage of neuronal cells was calculated over the total number of tdTomato and IRES-CFP-positive cells (Ctrl: n = 3, LB1 OE n = 3; paired t test).
(H) SUN1 protein levels decrease upon LB1 overexpression. Sections shown were stained against SUN1 (white), IRES-CFP (green), and tdTomato (red). Upper row shows control cells, and the lower row shows cells overexpressing LB1. SUN1 intensities were quantified in R cells that were IRES-CFP+ and tdTomato+ for both conditions in the 4-week cohort. Graphs indicate the fluorescence intensities in each cell in the two conditions (left; Ctrl: n = 45, LB1 OE: n = 34; mean ± SD; unpaired t test) and the average fluorescence intensities: per animal for each condition (right; Ctrl: n = 3, LB1 OE: n = 3; paired t test).
Scale bars represent 50 μm (A, B, and D), 25 μm (H), 10 μm (boxed D), and 5 μm (D–F). *$p < 0.05$; ***$p < 0.001$. See also Figure S4.

membrane barrier, which is associated with the asymmetric segregation of aging factors, such as damaged proteins in budding yeast, *C. elegans*, and NSCs (Lee et al., 2016; Moore et al., 2015; Shcheprova et al., 2008). Further, the asymmetric segregation of aging factors is correlated with proliferation capacity (Bufalino et al., 2013; Moore et al., 2015). Thus, a weakening of the ER barrier with age, as described before, may contribute to age-related proliferation deficits observed in aged NSCs. Supporting such a role for the ER barrier, we found that restoring LB1 levels in aged hippocampal progenitors increased Ub levels in NR cells, potentially by enhancing asymmetric segregation of Ub as suggested before (Moore et al., 2015). How LB1 and SUN1 contribute on a molecular level to the establishment or strengthening of the ER barrier remains unknown. However, it is interesting to note that components of the nuclear envelope, such as lamins, disperse into the ER and become integrated into the ER membrane during mammalian cell divisions, where they may contribute to barrier strength (Moir et al., 2000; Rabut et al., 2004). Future studies will be needed to understand the molecular underpinnings of the ER diffusion barrier and its exact role in stem cell aging.

We here show that re-expression of LB1 in aged progenitors is sufficient to increase proliferation and neurogenesis within the endogenous hippocampal niche. Thus, our data identify a novel mechanism of how cell-intrinsic, age-related alterations in NSCs affect their behavior and open up a novel route to target aging progenitors to ameliorate their function in the context of age-related disease.

Limitations of study

The mechanistic connection between age-related changes in protein levels of LB1/SUN1 and their effects on the strength of the ER-membrane diffusion barrier in young and aged proliferating progenitors remains at this point correlative. This is based on the current challenge to determine the strength of the ER-membrane diffusion barrier directly within neurogenic cells of the aged hippocampus *in vivo*. In addition, the detailed effects of LB1 and SUN1 on each developmental step from quiescent stem cells to maturing neurons will need to be further analyzed in future studies.

STAR★METHODS

Detailed methods are provided in the online version of this paper and include the following:

SUPPLEMENTAL INFORMATION

Supplemental information can be found online at https://doi.org/10.1016/j.stem.2021.01.015.

ACKNOWLEDGMENTS

We thank Y.H. Chi for sharing SUN1 antibodies, D.C. Lie for comments, and J.D. Cole and D. Wüthrich for experimental help. This work was supported by the European Research Council (STEMBAR to S.J.), the Swiss National Science Foundation (BSCGI0_157859 and 310030_196869 to S.J.), the Helmut Horten Foundation (to S.J.), the Wisconsin Partnership Program (to D.L.M.), a DP2 NIH New Innovator Award (to D.L.M.), and the Zurich Neuroscience Center (ZNZ).

AUTHOR CONTRIBUTIONS

M.K.b.I. performed experiments, analyzed data, and co-wrote the manuscript. B.N.J., S.B., R.A.C.M., and M.V. performed experiments. D.L.M. analyzed data, co-developed the concept, and revised the manuscript. S.J. developed the concept and wrote the manuscript.

DECLARATION OF INTERESTS

The authors declare no competing interests.

Received: January 16, 2020
Revised: November 19, 2020
Accepted: January 21, 2021
Published: February 24, 2021

REFERENCES

Ahn, S., and Joyner, A.L. (2005). In vivo analysis of quiescent adult neural stem cells responding to Sonic hedgehog. Nature *437*, 894–897.

Anacker, C., and Hen, R. (2017). Adult hippocampal neurogenesis and cognitive flexibility - linking memory and mood. Nat. Rev. Neurosci. *18*, 335–346.

Beckervordersandforth, R., Ebert, B., Schäffner, I., Moss, J., Fiebig, C., Shin, J., Moore, D.L., Ghosh, L., Trinchero, M.F., Stockburger, C., et al. (2017). Role of mitochondrial metabolism in the control of early lineage progression and aging phenotypes in adult hippocampal neurogenesis. Neuron *93*, 560–573.e6.

Ben Abdallah, N.M., Slomianka, L., Vyssotski, A.L., and Lipp, H.P. (2010). Early age-related changes in adult hippocampal neurogenesis in C57 mice. Neurobiol. Aging *31*, 151–161.

Bottes, S., Jaeger, B.N., Pilz, G.A., Jörg, D.J., Cole, J.D., Kruse, M., Harris, L., Korobeynyk, V.I., Mallona, I., Helmchen, F., et al. (2021). Long-term self-renewing stem cells in the adult mouse hippocampus identified by intravital imaging. Nat Neurosci *24*, 225–233.

Bracko, O., Singer, T., Aigner, S., Knobloch, M., Winner, B., Ray, J., Clemenson, G.D., Jr., Suh, H., Couillard-Despres, S., Aigner, L., et al. (2012). Gene expression profiling of neural stem cells and their neuronal progeny

reveals IGF2 as a regulator of adult hippocampal neurogenesis. J. Neurosci. *32*, 3376–3387.

Bufalino, M.R., DeVeale, B., and van der Kooy, D. (2013). The asymmetric segregation of damaged proteins is stem cell-type dependent. J. Cell Biol. *201*, 523–530.

Chen, C.Y., Chi, Y.H., Mutalif, R.A., Starost, M.F., Myers, T.G., Anderson, S.A., Stewart, C.L., and Jeang, K.T. (2012). Accumulation of the inner nuclear envelope protein Sun1 is pathogenic in progeric and dystrophic laminopathies. Cell *149*, 565–577.

Coffinier, C., Jung, H.J., Nobumori, C., Chang, S., Tu, Y., Barnes, R.H., 2nd, Yoshinaga, Y., de Jong, P.J., Vergnes, L., Reue, K., et al. (2011). Deficiencies in lamin B1 and lamin B2 cause neurodevelopmental defects and distinct nuclear shape abnormalities in neurons. Mol. Biol. Cell *22*, 4683–4693.

de Leeuw, R., Gruenbaum, Y., and Medalia, O. (2018). Nuclear lamins: thin filaments with major functions. Trends Cell Biol. *28*, 34–45.

Dobin, A., Davis, C.A., Schlesinger, F., Drenkow, J., Zaleski, C., Jha, S., Batut, P., Chaisson, M., and Gingeras, T.R. (2013). STAR: ultrafast universal RNA-seq aligner. Bioinformatics *29*, 15–21.

Drapeau, E., Mayo, W., Aurousseau, C., Le Moal, M., Piazza, P.V., and Abrous, D.N. (2003). Spatial memory performances of aged rats in the water maze predict levels of hippocampal neurogenesis. Proc. Natl. Acad. Sci. USA *100*, 14385–14390.

Ermolaeva, M., Neri, F., Ori, A., and Rudolph, K.L. (2018). Cellular and epigenetic drivers of stem cell ageing. Nat. Rev. Mol. Cell Biol. *19*, 594–610.

Goldman, R.D., Shumaker, D.K., Erdos, M.R., Eriksson, M., Goldman, A.E., Gordon, L.B., Gruenbaum, Y., Khuon, S., Mendez, M., Varga, R., and Collins, F.S. (2004). Accumulation of mutant lamin A causes progressive changes in nuclear architecture in Hutchinson-Gilford progeria syndrome. Proc. Natl. Acad. Sci. USA *101*, 8963–8968.

Gonçalves, J.T., Schafer, S.T., and Gage, F.H. (2016). Adult neurogenesis in the hippocampus: from stem cells to behavior. Cell *167*, 897–914.

Haque, F., Lloyd, D.J., Smallwood, D.T., Dent, C.L., Shanahan, C.M., Fry, A.M., Trembath, R.C., and Shackleton, S. (2006). SUN1 interacts with nuclear lamin A and cytoplasmic nesprins to provide a physical connection between the nuclear lamina and the cytoskeleton. Mol. Cell. Biol. *26*, 3738–3751.

Jaeger, B.N., Yángüez, E., Gesuita, L., Denoth-Lippuner, A., Kruse, M., Karayannis, T., and Jessberger, S. (2020). Miniaturization of Smart-seq2 for single-cell and single-nucleus RNA sequencing. STAR Protoc. *1*, 100081.

Jung, H.J., Coffinier, C., Choe, Y., Beigneux, A.P., Davies, B.S., Yang, S.H., Barnes, R.H., 2nd, Hong, J., Sun, T., Pleasure, S.J., et al. (2012). Regulation of prelamin A but not lamin C by miR-9, a brain-specific microRNA. Proc. Natl. Acad. Sci. USA *109*, E423–E431.

Kalamakis, G., Brüne, D., Ravichandran, S., Bolz, J., Fan, W., Ziebell, F., Stiehl, T., Catalá-Martinez, F., Kupke, J., Zhao, S., et al. (2019). Quiescence modulates stem cell maintenance and regenerative capacity in the aging brain. Cell *176*, 1407–1419.e14.

Katsimpardi, L., and Lledo, P.M. (2018). Regulation of neurogenesis in the adult and aging brain. Curr. Opin. Neurobiol. *53*, 131–138.

Katsimpardi, L., Litterman, N.K., Schein, P.A., Miller, C.M., Loffredo, F.S., Wojtkiewicz, G.R., Chen, J.W., Lee, R.T., Wagers, A.J., and Rubin, L.L. (2014). Vascular and neurogenic rejuvenation of the aging mouse brain by young systemic factors. Science *344*, 630–634.

Kempermann, G. (2015). Activity dependency and aging in the regulation of adult neurogenesis. Cold Spring Harb. Perspect. Biol. *7*, a018929.

Kempermann, G., Gast, D., and Gage, F.H. (2002). Neuroplasticity in old age: sustained fivefold induction of hippocampal neurogenesis by long-term environmental enrichment. Ann. Neurol. *52*, 135–143.

Knobloch, M., Pilz, G.A., Ghesquière, B., Kovacs, W.J., Wegleiter, T., Moore, D.L., Hruzova, M., Zamboni, N., Carmeliet, P., and Jessberger, S. (2017). A fatty acid oxidation-dependent metabolic shift regulates adult neural stem cell activity. Cell Rep. *20*, 2144–2155.

Kuhn, H.G., Dickinson-Anson, H., and Gage, F.H. (1996). Neurogenesis in the dentate gyrus of the adult rat: age-related decrease of neuronal progenitor proliferation. J. Neurosci. *16*, 2027–2033.

Larrieu, D., Britton, S., Demir, M., Rodriguez, R., and Jackson, S.P. (2014). Chemical inhibition of NAT10 corrects defects of laminopathic cells. Science *344*, 527–532.

Lee, Z.Y., Prouteau, M., Gotta, M., and Barral, Y. (2016). Compartmentalization of the endoplasmic reticulum in the early C. elegans embryos. J. Cell Biol. *214*, 665–676.

Leeman, D.S., Hebestreit, K., Ruetz, T., Webb, A.E., McKay, A., Pollina, E.A., Dulken, B.W., Zhao, X., Yeo, R.W., Ho, T.T., et al. (2018). Lysosome activation clears aggregates and enhances quiescent neural stem cell activation during aging. Science *359*, 1277–1283.

Liao, Y., Smyth, G.K., and Shi, W. (2013). The Subread aligner: fast, accurate and scalable read mapping by seed-and-vote. Nucleic Acids Res. *41*, e108.

Love, M.I., Huber, W., and Anders, S. (2014). Moderated estimation of fold change and dispersion for RNA-seq data with DESeq2. Genome Biol. *15*, 550.

Mahajani, S., Giacomini, C., Marinaro, F., De Pietri Tonelli, D., Contestabile, A., and Gasparini, L. (2017). Lamin B1 levels modulate differentiation into neurons during embryonic corticogenesis. Sci. Rep. *7*, 4897.

Martynoga, B., Mateo, J.L., Zhou, B., Andersen, J., Achimastou, A., Urbán, N., van den Berg, D., Georgopoulou, D., Hadjur, S., Wittbrodt, J., et al. (2013). Epigenomic enhancer annotation reveals a key role for NFIX in neural stem cell quiescence. Genes Dev. *27*, 1769–1786.

Mattioli, E., Columbaro, M., Capanni, C., Maraldi, N.M., Cenni, V., Scotlandi, K., Marino, M.T., Merlini, L., Squarzoni, S., and Lattanzi, G. (2011). Prelamin A-mediated recruitment of SUN1 to the nuclear envelope directs nuclear positioning in human muscle. Cell Death Differ. *18*, 1305–1315.

Meng, D., Frank, A.R., and Jewell, J.L. (2018). mTOR signaling in stem and progenitor cells. Development *145*, dev152595.

Miller, J.D., Ganat, Y.M., Kishinevsky, S., Bowman, R.L., Liu, B., Tu, E.Y., Mandal, P.K., Vera, E., Shim, J.W., Kriks, S., et al. (2013). Human iPSC-based modeling of late-onset disease via progerin-induced aging. Cell Stem Cell *13*, 691–705.

Mira, H., Andreu, Z., Suh, H., Lie, D.C., Jessberger, S., Consiglio, A., San Emeterio, J., Hortigüela, R., Marqués-Torrejón, M.A., Nakashima, K., et al. (2010). Signaling through BMPR-IA regulates quiescence and long-term activity of neural stem cells in the adult hippocampus. Cell Stem Cell *7*, 78–89.

Moir, R.D., Spann, T.P., Lopez-Soler, R.I., Yoon, M., Goldman, A.E., Khuon, S., and Goldman, R.D. (2000). Review: the dynamics of the nuclear lamins during the cell cycle– relationship between structure and function. J. Struct. Biol. *129*, 324–334.

Moore, D.L., Pilz, G.A., Araúzo-Bravo, M.J., Barral, Y., and Jessberger, S. (2015). A mechanism for the segregation of age in mammalian neural stem cells. Science *349*, 1334–1338.

Morrow, C.S., Porter, T.J., Xu, N., Arndt, Z.P., Ako-Asare, K., Heo, H.J., Thompson, E.A.N., and Moore, D.L. (2020). Vimentin coordinates protein turnover at the aggresome during neural stem cell quiescence exit. Cell Stem Cell *26*, 558–568.e9.

Obernier, K., and Alvarez-Buylla, A. (2019). Neural stem cells: origin, heterogeneity and regulation in the adult mammalian brain. Development *146*, dev156059.

Rabut, G., Lénárt, P., and Ellenberg, J. (2004). Dynamics of nuclear pore complex organization through the cell cycle. Curr. Opin. Cell Biol. *16*, 314–321.

Scaffidi, P., and Misteli, T. (2008). Lamin A-dependent misregulation of adult stem cells associated with accelerated ageing. Nat. Cell Biol. *10*, 452–459.

Schreiber, K.H., and Kennedy, B.K. (2013). When lamins go bad: nuclear structure and disease. Cell *152*, 1365–1375.

Seib, D.R., Corsini, N.S., Ellwanger, K., Plaas, C., Mateos, A., Pitzer, C., Niehrs, C., Celikel, T., and Martin-Villalba, A. (2013). Loss of Dickkopf-1 restores neurogenesis in old age and counteracts cognitive decline. Cell Stem Cell *12*, 204–214.

Shcheprova, Z., Baldi, S., Frei, S.B., Gonnet, G., and Barral, Y. (2008). A mechanism for asymmetric segregation of age during yeast budding. Nature *454*, 728–734.

Shimi, T., Butin-Israeli, V., Adam, S.A., Hamanaka, R.B., Goldman, A.E., Lucas, C.A., Shumaker, D.K., Kosak, S.T., Chandel, N.S., and Goldman, R.D. (2011). The role of nuclear lamin B1 in cell proliferation and senescence. Genes Dev. *25*, 2579–2593.

Shitamukai, A., Konno, D., and Matsuzaki, F. (2011). Oblique radial glial divisions in the developing mouse neocortex induce self-renewing progenitors outside the germinal zone that resemble primate outer subventricular zone progenitors. J. Neurosci. *31*, 3683–3695.

Silva-Vargas, V., Maldonado-Soto, A.R., Mizrak, D., Codega, P., and Doetsch, F. (2016). Age-dependent niche signals from the choroid plexus regulate adult neural stem cells. Cell Stem Cell *19*, 643–652.

Stankovic, A., Guo, L.Y., Mata, J.F., Bodor, D.L., Cao, X.J., Bailey, A.O., Shabanowitz, J., Hunt, D.F., Garcia, B.A., Black, B.E., and Jansen, L.E.T. (2017). A dual inhibitory mechanism sufficient to maintain cell-cycle-restricted CENP-A assembly. Mol. Cell *65*, 231–246.

Starr, D.A. (2012). Laminopathies: too much SUN is a bad thing. Curr. Biol. *22*, R678–R680.

Starr, D.A., and Fridolfsson, H.N. (2010). Interactions between nuclei and the cytoskeleton are mediated by SUN-KASH nuclear-envelope bridges. Annu. Rev. Cell Dev. Biol. *26*, 421–444.

Stuart, T., Butler, A., Hoffman, P., Hafemeister, C., Papalexi, E., Mauck, W.M., 3rd, Hao, Y., Stoeckius, M., Smibert, P., and Satija, R. (2019). Comprehensive integration of single-cell data. Cell *177*, 1888–1902.e21.

Takamori, Y., Tamura, Y., Kataoka, Y., Cui, Y., Seo, S., Kanazawa, T., Kurokawa, K., and Yamada, H. (2007). Differential expression of nuclear lamin, the major component of nuclear lamina, during neurogenesis in two germinal regions of adult rat brain. Eur. J. Neurosci. *25*, 1653–1662.

Tapley, E.C., and Starr, D.A. (2013). Connecting the nucleus to the cytoskeleton by SUN-KASH bridges across the nuclear envelope. Curr. Opin. Cell Biol. *25*, 57–62.

Toda, T., Hsu, J.Y., Linker, S.B., Hu, L., Schafer, S.T., Mertens, J., Jacinto, F.V., Hetzer, M.W., and Gage, F.H. (2017). Nup153 interacts with Sox2 to enable bimodal gene regulation and maintenance of neural progenitor cells. Cell Stem Cell *21*, 618–634.e7.

Tsai, M.-Y., Wang, S., Heidinger, J.M., Shumaker, D.K., Adam, S.A., Goldman, R.D., and Zheng, Y. (2006). A mitotic lamin B matrix induced by RanGTP required for spindle assembly. Science *311*, 1887–1893.

van Praag, H., Shubert, T., Zhao, C., and Gage, F.H. (2005). Exercise enhances learning and hippocampal neurogenesis in aged mice. J. Neurosci. *25*, 8680–8685.

Villeda, S.A., Luo, J., Mosher, K.I., Zou, B., Britschgi, M., Bieri, G., Stan, T.M., Fainberg, N., Ding, Z., Eggel, A., et al. (2011). The ageing systemic milieu negatively regulates neurogenesis and cognitive function. Nature *477*, 90–94.

Ziebell, F., Dehler, S., Martin-Villalba, A., and Marciniak-Czochra, A. (2018). Revealing age-related changes of adult hippocampal neurogenesis using mathematical models. Development *145*, dev153544.

Joshi, N., and Fass, J. (2011). Sickle: A sliding-window, adaptive, quality-based trimming tool for FastQ files (Version 1.33) [Software]. Available at https://Github.Com/Najoshi/Sickle.

Please cite this article in press as: bin Imtiaz et al., Declining lamin B1 expression mediates age-dependent decreases of hippocampal stem cell activity, Cell Stem Cell (2021), https://doi.org/10.1016/j.stem.2021.01.015

STAR★METHODS

KEY RESOURCES TABLE

REAGENT/RESOURCE	SUPPLIER/SOURCE	PRODUCT IDENTIFIER
Antibodies		
Rabbit α-LaminB1 (1:500 for sections, 1:1000 for cells)	Abcam	Cat# ab16048; RRID: AB_10107828
Rabbit α-SUN1 (1:500)	Chen et al., 2012	PMID: 22541428
Goat α-GFP (1:500 for sections, 1:1000 for cells)	Rockland	Cat#600-101-215; RRID: AB_218182
Chicken α-GFP (1:500 for sections, 1:1000 for cells)	Aves	Cat#GFP.1020; RRID: AB_10000240
Guinea pig α-DCX (1:500)	Millipore	Cat# ab2253; RRID: AB_1586992
Mouse α mono and poly ubiquitin (FK2) (1:100)	Enzo Life Sciences	Cat# BML-PW8810-0500; RRID: AB_2051891
Rat α-Sox2 (1:500)	ebiosciences	Cat# 14-9811-82; RRID:AB_11219471
Rat α-Ki67 (1:500)	ebiosciences	Cat# 14-5698-82; RRID: AB_10854564
Chicken α-GFAP (1:500)	Aves	Cat# GFAP; RRID: AB_2313547
Mouse α-Lamin A/C	CIND	Cat# MANLAC1; RRID: AB_2618203
Mouse α-Lamin B2 (1:50)	Invitrogen	Cat# 33-2100; RRID: AB_2533107
AffiniPure Donkey α-rabbit IgG(H+L) Antibody coupled to different fluorophores	Jackson Immuno Research Labs	Cat#711-005-152; RRID: AB_2340585
AffiniPure Donkey α-goat IgG(H+L) Antibody coupled to different fluorophores	Jackson Immuno Research Labs	Cat#705-005-147; RRID: AB_2340385
AffiniPure Donkey α-rat IgG(H+L) Antibody coupled to different fluorophores	Jackson Immuno Research Labs	Cat#712-005-150; RRID: AB_2340630
AffiniPure Donkey α-chicken IgG(H+L) Antibody coupled to different fluorophores	Jackson Immuno Research Labs	Cat# 703-005-155; RRID: AB_2340346
AffiniPure Donkey α-guinea pig IgG(H+L) Antibody coupled to different fluorophores	Jackson Immuno Research	Cat# 706-605-148; RRID: AB_2340476
Chemicals, peptides, and recombinant proteins		
XbaI	New England Biolabs	Cat# R0145
BamHI-HF	New England Biolabs	Cat# R3136
AgeI-HF	New England Biolabs	Cat# R3552
SalI-HF	New England Biolabs	Cat# R0138
SfiI	New England Biolabs	Cat# R0123
Agencourt AMPure XP beads	Beckman Coulter	Cat# B37419AA
Superscript II	Life Technologies	Cat# 18064014
B27-Supplement	Thermo Fisher Scientific	Cat# 17504044
EGF	PeproTech	Cat# AF-100-15
FGF-2	PeproTech	Cat# 100-18B
DMEM/F-12 GlutaMAX	Thermo Fisher Scientific	Cat# 31331028
Poly-L-ornithine	Sigma Aldrich	Cat# P3655
poly-D-lysine	Sigma Aldrich	Cat# P6407
Laminin	Sigma-Aldrich	Cat# L2020
Mouse BMP4	R&D Systems	Cat# 5020-BP-010
Gibson Assembly Master Mix	New England Biolabs	Cat# E2611

(*Continued on next page*)

Please cite this article in press as: bin Imtiaz et al., Declining lamin B1 expression mediates age-dependent decreases of hippocampal stem cell activity, Cell Stem Cell (2021), https://doi.org/10.1016/j.stem.2021.01.015

Continued

REAGENT/RESOURCE	SUPPLIER/SOURCE	PRODUCT IDENTIFIER
Phusion Polymerase	New England Biolabs	Cat# M0530
T4 DNA Ligase	New England Biolabs	Cat# M0202
Ethanol	VWR Chemicals	Cat# 20821.321
Puromycin	GIBCO	Cat# A111380-03
Lipofectamine 2000 Transfection Reagent	Thermo Fisher Scientific	Cat# 11668027
5-ethynyl-2′-deoxyuridine (EdU)	Thermo Fisher Scientific	Cat# E10415
EDTA	Sigma-Aldrich	Cat# EDS
Paraformaldehyde	Sigma Aldrich	Cat# 441244
4',6-diamidino-2-phenylindole (DAPI)	Sigma Aldrich	Cat# D9542
β- Mercaptoethanol	Thermo Fisher Scientific	Cat# 31350-010
DPBS	Thermo Fisher Scientific	Cat# 14190-094
PBS	Thermo Fisher Scientific	Cat# 10010-015
0.5M EDTA Trypsin	Thermo Fisher Scientific	Cat# 25300054
Triton X-100	Sigma Aldrich	Cat# 93443
Tamoxifen	Sigma Aldrich	Cat# T5648
Corn oil	Sigma Aldrich	Cat# 8267
Sucrose	Sigma Aldrich	Cat# 84100
ImmuMount	Thermo Fisher Scientific	Cat# 9990402
Donkey Serum	Millipore	Cat# 530
Trypsin (2.5%)	Thermo Fisher Scientific	Cat# 15090046
Trypsin Inhibitor	Sigma Aldrich	Cat# T6522-100MG
Commercial kits		
KAPA Hifi HotStart ReadyMix	Roche	Cat# KK2602
D1000 Screen Tape Assay	Agilent Technologies	N/A
Nextera XT DNA Library Preparation Kit	Illumina	Cat# FC-131-1096
PureLink RNA Mini Kit	Thermo Fisher Scientific	Cat# 12183020
Click-iT EdU Alexa Fluor 647 Imaging Kit	Thermo Fisher Scientific	Cat# C10340
QIAquick Gel Extraction Kit	QIAGEN	Cat# 28706
QIAprep Spin Miniprep Kit	QIAGEN	Cat# 27106
MACS Neural Tissue Dissociation Kit (P)	Miltenyl Biotec	Cat# 130-092-628
NucleoSpin Plasmid	Macherey-Nagel	Cat# 740588.250
PureLine Expi Plasmid Purification Kit	Thermo Fisher Scientific	Cat# A31231
Oligonucleotides		
Reverse primer to amplify LB1 cDNA 5′-TGA GCA GCC CGA GAG GAA AC-3′		N/A
Forward primer to amplify LB1 cDNA 5′-TGA GCA GCC CGA GAG GAA AC-3′		N/A
Forward primer to amplify SUN1 cDNA 5′- CGG GA T CCG CCG CCA CCA TGG ACT TTT CTC GGC T-3′		N/A
Reverse primer to amplify SUN1 cDNA 5′- CCA CGG AGA GCC CAT CCA GTA GGG ATC CCG C-3′		N/A
Forward sequencing primer for CAG-GFP plasmid 5′-TGG CAA AGA ATT CGC TAG- 3′		N/A
Reverse sequencing primer for CAG-GFP plasmid 5′-CAG AGG TTG ATT GGT TTA AAC −3′		N/A
Forward primer to amplify loxP-STOP-loxP cassette 5′- TCA TTT TGG CAA AGA ATT −3′		N/A

(*Continued on next page*)

Please cite this article in press as: bin Imtiaz et al., Declining lamin B1 expression mediates age-dependent decreases of hippocampal stem cell activity, Cell Stem Cell (2021), https://doi.org/10.1016/j.stem.2021.01.015

Continued

REAGENT/RESOURCE	SUPPLIER/SOURCE	PRODUCT IDENTIFIER
Reverse primer to amplify loxP-STOP-loxP cassette 5′ - ATA ACT TCG TAT AAT GTA TG −3′		N/A
Forward primer to genotype Gli1-Cre mice 5′- TAA AGA TAT CTC ACG TAC TGA CGG TG-3′		N/A
Reverse primer to genotype Gli1-Cre mice 5′- TCT CTG ACC AGA GTC ATC CTT AGC-3′		N/A
Forward primer to sequence pLenti plasmid 5′-CTC CTC ATA AAG AGA CAG-3′		N/A
Reverse primer to sequence pLenti plasmid 5′-AGT CTC CAC CCC ATT GAC-3′		N/A
Software and programs		
ZEN Blue	Carl Zeiss	http://www.zeiss.com RRID: SCR_013672
Fiji/ImageJ	Fiji	https://fiji.sc RRID:SCR_002285
GraphPad Prism	GraphPad	https://graphpad.com:443/ RRID:SCR_002798
ApE Plasmid Editor	M. Wayne Davis	https://biologylabs.utah.edu/jorgensen/wayned/ape RRID:SCR_014266
Sushi analysis pipeline	Functional Genomics Center Zurich	https://fgcz-sushi.uzh.ch/users/sign_in
Cutadapt v2.10		https://doi.org/10.14806/ej.17.1.200
Sickle v1.33	Joshi and Fass, 2011	https://github.com/najoshi/sickle
Subread v1.6.3	Liao et al., 2013	PMC3664803
Seurat v3.0	Stuart et al., 2019	PMC6687398
DESeq2 v1.30.0	Love et al., 2014	PMC4302049
Recombinant DNA		
CAG-GFP	Addgene	Cat# 16664; RRID:Addgene_16664
Progerin	Addgene	Cat# 17663; RRID:Addgene_17663
Sec61β	Addgene	Cat# 15108; RRID:Addgene_15108
pLenti-CMV-GFP-Hygro	Addgene	Cat# 17446; RRID:Addgene_17446
pCas9-2A-Puro	Addgene	Cat# PX459; RRID:Addgene_48139
MGC Mouse SUN1 cDNA	GE Healthcare	Cat# 5321879
Sel1L	A gift from M. Molinari	N/A
Sec61α-GFP	A gift from A. Helenius	N/A
pUEG	A gift from Hongjun Song's lab	N/A
Deposited data		
RNA-seq data available at GEO under the accession number GEO: GSE163795	This paper	https://www.ncbi.nlm.nih.gov/geo/query/acc.cgi?acc=GSE163795
Other		
LSM 800 Confocal Microscope	Carl Zeiss	N/A
Nunc Lab-Tek 4-well chambered coverglass	Thermo Fisher Scientific	Cat# 155382
Leica TCS SP8	Leica Microsystems	N/A
Illumina NovaSeq 6000	Illumina	N/A

RESOURCE AVAILABILITY

Lead contact

Further information and requests for resources and reagents should be directed to and will be fulfilled by the lead contact, Sebastian Jessberger (jessberger@hifo.uzh.ch).

Materials availability

Genetic markers of the endoplasmic reticulum and gain- and loss-of-function constructs for LB1 and SUN1 will be provided directly. Materials will be provided upon execution of a suitable Materials Transfer Agreement.

Data and code availability

All data are available from the authors at request. The accession number for the RNA-seq data reported in this paper is GEO: GSO163795 (https://www.ncbi.nlm.nih.gov/geo/query/acc.cgi?acc=GSE163795).

EXPERIMENTAL MODEL AND SUBJECT DETAILS

Animals

The mice used in this study were kept in a specific pathogen free (SPF) animal facility according to the guidelines of the Federation of European Laboratory Animal Science Associations (FELASA) and were kept with littermates under a 12h dark/light cycle. The mice were housed in individually ventilated cages (21-23°C) and with *ad libitum* access to food and water. The persons entering the facility were obliged to wear protective clothing, facemasks, hairnets and gloves to ensure the pathogen free environment. The *Gli1-Cre^{ERT2};tdTomato* mice were generated by crossing Gli1-CreERT2 mice (Gli1$^{tm3(cre/ERT2)Alj}$; The Jackson Laboratory 007913) with homozygous CAG tdTomato (Ai14;B6.Cg-GT(ROSA)$^{26Sortm14(CAG-tdTomato)Hze}$; The Jackson Laboratory, 007914). The genetic background of the mouse line was confirmed by sequencing of analysis of 2,050 single-nucleotide polymorphisms (Biolytix) and compared to results from C57BL/6 and 129S control animals where the mouse line showed an overlap of 91.5% (C57BL/6) and 46.7% (129S). The animals used in this study were not subjected to any previous tests or procedures. The mice were genotyped using 5′-TAA AGA TAT CTC ACG TAC TGA CGG TG-3′ forward and 5′- TCT CTG ACC AGA GTC ATC CTT AGC-3′ reverse primers. All animal experiments were performed according to Swiss regulatory standards and approved by the Veterinary office of the Canton of Zurich.

Primary Cell Culture

Primary NSCs were isolated from young (6 week old) and aged/old (9 month old) B6/J-Rj (Janvier) male mice simultaneously as previously described (Moore et al., 2015). In summary, after hippocampal isolation and processing, the cells were cultured in DMEM/DMEM/F12 media containing PSF (Invitrogen), supplemented with B27 (Thermo Fisher Scientific), and growth factors EGF/FGF (PeproTech; both 20ng/ml).

METHOD DETAILS

Mouse neural stem cell cultures

Six weeks and 9-month-old mice were used to isolate NSCs (named: young and aged/old cells), respectively. After cervical dislocation, hippocampi were isolated. The tissue was dissociated using the Miltenyl gentleMACS Dissociator and MACS Neural Tissue Dissociation Kit (P) (Miltenyl Biotec) according to the manufacturer's protocol. Cells were then plated in DMEM/F12 media containing PSF (Invitrogen), supplemented with B27 (Thermo Fisher Scientific), and growth factors EGF/FGF (PeproTech; both 20ng/ml). Media was changed every 2 days. To obtain a NSC population, cells were allowed to make primary and secondary neurospheres, which were then spun down and dissociated using trypsin (Thermo Fisher Scientific) and trypsin inhibitor (Sigma Aldrich) (Moore et al., 2015). Old and young NSCs were both isolated at the same time and proliferation assays were performed after both had formed primary and secondary neurospheres (approximately 12 days for young and 20 days for old NSCs). All experiments where young and old NSCs are compared were performed with comparable days *in vitro* (DIV). Old cells were not used beyond 60 DIV. No experiments were performed when the proliferation of old NSCs matched the proliferation of young NSCs. For proliferation assays, wells in a 12 well plate were first coated with Poly-L-ornithine (Sigma Aldrich) for 1 hour at 37°C and then overnight with Laminin at 4°C. 30,000 NSCs were then seeded on the coated wells. Two days after plating, 5-ethynyl-2′-deoxyuridine (EdU) was added to the wells (final concentration 10μm) and the NSCs were incubated for 1 hour at 37°C. The plates were then fixed with 4% PFA (Sigma Aldrich) for 15 mins at room temperature before being washed with PBS. After fixation, the cells were blocked and permeabilized with 3% donkey serum (Millipore) and 0.25% Triton X-100 (Sigma Aldrich) in TBS for 30 mins at room temperature. EdU was then labeled fluorescently with the EdU Click-it Assay with AlexaFlour 647 (Thermo Fisher Scientific) following the protocol provided by the manufacturer. All nuclei were then labeled with DAPI. 3 wells were then imaged under a 20x objective to quantify the proliferation. The number of DAPI and EdU cells were counted and then analyzed. For cell cycle analyses EdU and DAPI were measured in stained nuclei. Cells positive for EdU were identified and the mean and standard deviation of their DAPI intensities were calculated. Standard deviation was subtracted from the mean to obtain the threshold below which the nuclei were identified as G1. Nuclei above this

threshold were identified as G2. For LB1 knockout cells, $4x10^6$ were electroporated with 2μg of the plasmid. The cells were plated in plates coated with poly-L-ornithine (Sigma-Aldrich) and Laminin (Sigma-Aldrich) for 1 day before they were subjected to selection by puromycin (Thermofisher) with the final concentration of 0.7μg/ml. The cells were selected for 48 hours. Following this, colonies were made and then immunostained to confirm a full knockout. Colonies with full knockout were selected for the FLIP assays. The control condition underwent the same treatment. To induce quiescence, cells were plated in DMEM/F12 media containing PSF (Invitrogen), supplemented with B27 (Thermo Fisher Scientific), FGF (20ng/μl) and BMP4 (50ng/ml). Cells were incubated with this media for 3 days. To measure quiescence induction, cells were plated in this media for 2 days.

Stereotactic lentivirus Injections

To generate Gli1CreER^{T2}/tdTom mice (Gli1Cre ± Ai14+/−), Gli1CreER^{T2} mice (Gli1$^{tm3(cre/ERT2)Alj}$, Jackson lab strain 007913) were crossed to homozygous CAG tdTomato (Ai14; B6.Cg-Gt(ROSA)$^{26Sortm14(CAG-tdTomato)Hze}$; JacksonLab strain 007914) reporter strain (Ahn and Joyner, 2005). 6-month-old Gli1-CreERT^2-tdTom mice were used. Viruses were delivered to dentate gyri of 6-month-old (cohort 1) and 7-month- old (cohort 2) mice by stereotaxic injection of 1.5 μL of a solution of lentiviruses diluted in PBS. Mice were anaesthetized with isoflurane (1.5%–2% in O2) and positioned in a stereotaxic frame where the body temperature was measured and kept at 37°C with a heating pad. The skin was opened and a hole in the cranial bone was performed above the dorsal DG (coordinates: –2.0 posterior / ± 1.5 lateral mm from Bregma). The viruses were injected with a 5 μL Hamilton syringe at the depth of 2.3 mm from the skull surface. The LB1 overexpressing virus was injected in the left DG. The control virus was injected in the right DG. Two days after lentivirus injections, 180mg/kg of Tamoxifen (Sigma Aldrich) (Tam, diluted in cornoil (Sigma Aldrich) 100mg/5ml) was injected over three days intraperitoneally. Mice were perfused with 4% PFA 2 weeks and 4 weeks after the last Tam injection. All animal experiments were approved by the Cantonal Commission for Animal Experimentation of the Canton of Zurich, Switzerland in accordance with national and cantonal regulations.

Constructs and Cloning

Partial Sel1L sequence (corresponding to amino acids 178-310 from AAH57452.1; gift from M. Molinari) and Sec61β were cloned into a GFP-expressing vector as described before for Sec61α-sfGFP plasmid (Moore et al., 2015). Progerin and IRES-CFP constructs were used as described (Moore et al., 2015). LB1 cDNA was isolated from NSCs and total RNA extraction was performed using the PureLink RNA Mini Kit (Thermo Fisher Scientific). LB1 cDNA was then amplified using the primers 5′-TGA GCA GCC CGA GAG GAA AC-3′ (Forward) and 5′-TGA GCA GCC CGA GAG GAA AC-3′ (Reverse) and cloned into the CAG-IRES-CFP with retrovirus backbone overexpression construct using Gibson Assembly. For the SUN1 overexpression plasmid, SUN1 cDNA was isolated and amplified from the MGC Mouse SUN1 cDNA (GE Healthcare) using the primers 5′- CGG GA T CCG CCG CCA CCA TGG ACT TTT CTC GGC T-3′ (Forward) and 5′- CCA CGG AGA GCC CAT CCA GTA GGG ATC CCG C-3′ (Reverse) and then cloned into the CAG-IRES-CFP with retrovirus backbone overexpression construct using BamH1 restriction site. The plasmid was sequenced with 5′-TGG CAA AGA ATT CGC TAG-3′ (Forward) and 5′-CAG AGG TTG ATT GGT TTA AAC-3′ (Reverse). For the SUN1 knock-down plasmid, shRNA targeting SUN1 sequence 5′-AGG CTA TTG ATT CGC ACA TTA-3′ was designed and cloned into the pUEG plasmid (a gift from Hongjun Song's lab). For the control plasmid, a non-targeting, scrambled shRNA (5′-CCT AAG GTT AAG TCG CCC T-3′) was cloned into the pUEG plasmid. For LB1 knockout using CRISPR-Cas9, exon 4 of the LB1 gene was targeted (5′-GCG GGA GCA GCA CGA CGC GC-3′). For control, an empty CRISPR-Cas9 plasmid was used. The LB1 cDNA construct was also cloned into the pLenti CMV GFP Hygro plasmid (Addgene). For this cloning, loxP-STOP-loxP was isolated from the CAG FloxP mKO2 plasmid using PCR (Forward 5′- TCA TTT TGG CAA AGA ATT −3′; Reverse 5′-ATA ACT TCG TAT AAT GTA TG-3′) (Shitamukai et al., 2011). LoxP-STOP-loxP with LB1 IRES CFP was then cloned into the pLenti-CMV-GFP-Hygro in place of the GFP using Gibson Assembly. In the control plasmid, loxP-STOP-loxP was followed by IRES-CFP. Lentiviral particles were produced in HEK293T cells, which were co-transfected with pMDL, pREV and pVSVG. Virus particles were then isolated and enriched with high-speed centrifugation.

Image Analysis

For analyzing the fluorescence intensities of LB1 and SUN1 in cultured NSCs and brain sections, ImageJ was used. For cultured NSCs, fluorescence signal in each nucleus was measured in young and old NSCs. For progerin-IRES-CFP and IRES-CFP transduced NSCs, fluorescence signal in the IRES-CFP positive nucleus was measured and normalized to non-transduced NSCs in the coverslip. For brain sections, fluorescence signal of LB1 and SUN1 were measured in R, NR, IN and N nuclei as defined by their morphology and marker. These were then normalized to the background fluorescence of the tissue, i.e., fluorescence in the area where there are no cells present. For ubiquitin analysis, cells were identified based on their morphology and the total ubiquitin intensities were measured in area marked by tdTomato and IRES-CFP for the cell body and then normalized to the area of the cells. They were then normalized to the background ubiquitin intensity. Ubiquitin levels were not measured in the processes

Fluorescence Loss in Photobleaching (FLIP)

NSCs were plated in Poly-L-ornithine (Sigma Aldrich) and Laminin (Sigma Aldrich) coated Chambered Coverglass wells (Thermo Fisher Scientific). 63x oil objective in the Zeiss LSM 800 was used for live imaging and Fluorescence Loss In Photobleaching (FLIP) experiments. The wells were scanned visually to detect NSCs undergoing mitosis under brightfield. Then the NSCs detected were checked for the ER membrane marker-sfGFP and for H2B-mCherry or IRES-CFP fluorescence. Once the NSCs entered anaphase, a region in the Endoplasmic Reticulum (ER) close to the future cleavage furrow was bleached continuously with a

488nm laser at 3% power with 80 iterations. Images in a single plane were acquired before the bleaching started and then at intervals of 12 s, during which the bleaching was performed. A 488nm laser was used to acquire these images using between 2% and 4% laser power depending on the intensity of the fluorescence signal. The NSCs were bleached until no GFP was visible in the midbody. Following the FLIP experiment, a z stack was acquired. H2B-mCherry and IRES-CFP signals were also confirmed following the FLIP experiment. To analyze the loss in fluorescence, ImageJ was used to draw regions around the two compartments (bleached and unbleached) of a dividing cell and fluorescence intensity and area in each image was measured. Background fluorescence was also measured. Fluorescence intensities were divided by the area and then the background was subtracted. The bleached and unbleached fluorescence were normalized to the pre-bleach image for their respective compartments (initial picture was ascribed 100%). The normalized intensities for both compartments of all cells were averaged for each frame. To calculate barrier strength, fluorescence intensities from the bleached and the unbleached compartment were plotted on a graph in Prism. A one-phase decay curve was fitted to both with the following constraints: Plateau = 0, Y0 = 100, and K > 0. The value of K was then substituted into the following equation to obtain the time (t) it takes for the bleached and the unbleached intensities to fall to 80% from the initial 100%.

$$t80 = \frac{\ln\left(\frac{Y-Plateau}{YO-Plateau}\right)}{-K}$$

Where Y is 80 and K is derived from the fit from Prism.

For the Barrier Strength, the following equation was then used.

$$Barrier\ Strength = \frac{t_{Unbleached}}{t_{Bleached}}$$

Where the respective t80 values had been calculated above.

For the standard error in each half, the following equation was used.

$$Standard\ Error\ for\ each\ half = -seK \times \frac{\ln\left(\frac{Y-Plateau}{YO-Plateau}\right)}{K^2}$$

Where seK is the standard error of the constant K, derived from Prism.

For the total standard error, the following equations were used.

$$Barrier\ Index\ Standard\ Error_{Bleached} = t_{Unbleached} \times \frac{total\ error\ for\ Bleached}{t^2_{Bleached}}$$

$$Barrier\ Index\ Standard\ Error_{Unbleached} = \frac{total\ error\ Unbleached}{t_{Bleached}}$$

$$Standard\ Error\ in\ Barrier\ Strength = Barrier\ Strength\ S.E_{Bleached} + Barrier\ Strength\ S.E_{Unbleached}$$

This analysis has been previously described (Moore et al., 2015).

Analysis of brain sections

The brains were sectioned into 40μm thick sections and serially distributed in 12 tubes. The sections were then stained as outlined above. Sections with a minimum distance of 40μm (anterior and posterior) from the injection sites were analyzed. Sections that displayed damage because of the injection were not analyzed. The morphologies of each cell type were identified as follows; R cells were identified with their radial process, NR cells were identified by their lack of a radial process and N cells were identified by a clear apical dendrite extending into the molecular layer and the circular cell body. The fluorescence in the tdTomato and the IRES-CFP channels were used to identify the morphology.

Proliferation Assays

Wells in a 12 well plates were coated with Poly-L-ornithine (Sigma Aldrich) for 1 hour at 37°C and then overnight with Laminin at 4°C. 30,000 NSCs were then seeded on the coated wells. Two days after plating, 5-ethynyl-2′-deoxyuridine (EdU) was added to the wells (final concentration 10μM) and the NSCs were incubated for 1 hour at 37°C. The plates were then fixed with 4% PFA (Sigma Aldrich) for 15 mins before being washed with PBS. After fixation, the cells were blocked and permeabilized with 3% donkey serum (Millipore) and 0.25% Triton X-100 (Sigma Aldrich) in TBS for 30 mins at room temperature. EdU was then labeled fluorescently with the EdU Click-it Assay with AlexaFlour 647 (Thermo Fisher Scientific) following the protocol provided by the manufacturer. All nuclei were then labeled with DAPI. Three wells were then imaged under a 20x objective to quantify the proliferation. The number of DAPI and EdU cells were counted and then analyzed. For cell cycle analyses EdU and DAPI were measured in stained nuclei. Cells positive for EdU were identified and the mean and standard deviation of their DAPI intensities were calculated. Standard deviation was

subtracted from the mean to obtain the threshold below which the nuclei were identified as G1. Nuclei above this threshold were identified as G2, as described before (Stankovic et al., 2017).

Immunofluorescence

For immunostaining of cells, 90,000 NSCs were seeded on Poly-L-ornithine (Sigma Aldrich) and Laminin (Sigma Aldrich) coated coverslips. They were then fixed with 4% Paraformaldehyde (Sigma Aldrich) for 15 mins at room temperature. NSCs used for staining against LA/C were fixed with acetone/methanol (1:1) at −20°C for 20min. 3% Donkey Serum (Millipore) and 0.20% Triton X-100 (Sigma Aldrich) was used to block and permeabilize the cells for 1 hour. Different combinations of the following primary antibodies were then used: Rabbit anti LaminB1 (1:1000 Abcam), Rabbit α-SUN1 (1:500 (Chen et al., 2012), Goat α-GFP (1:1000, Rockland), Chicken α-GFP (1:1000 Aves). The coverslips were incubated overnight at 4°C in the primary antibodies. They were then washed thrice with TBS before being blocked again for 1 hour. Then, the coverslips were incubated with secondary antibodies at room temperature for 2 hours. They were then stained against DAPI and washed again with TBS. The coverslips were then mounted with ImmuMount (Thermo Fisher Scientific). For immunostainings of brain sections, mice were first perfused with 4% PFA (Sigma Aldrich). The brains were then isolated and left in the 4% PFA overnight. Next day, the brains were switched to 30% sucrose in PBS until they sank to the bottom of the tube. The brains were then sectioned into 40μm free-floating sections. They were then washed thrice with TBS and then blocked and permeabilized with TBS containing 3% Donkey Serum (Millipore) and 0.25% Triton X-100 (Sigma Aldrich) for 1 hour. Following this, the sections were incubated with the following primary antibodies for two nights at 4°C: rabbit α-LaminB1 (1:500, Abcam), rabbit α-SUN1 (1:500), goat α-GFP (1:500, Rockland), guinea pig α-DCX (1:500, Millipore), chicken α-GFAP (1:500, Aves), rat α-Ki67 (1:500, ebiosciences), rat α-Sox2 (1:500, ebiosciences), mouse α-ubiquitin (1:100, Enzo). The sections were washed again with TBS before being blocked prior to incubation with the secondary antibodies for 2 hours. They were then stained against DAPI and mounted on slides using ImmuMount (Thermo Fisher Scientific).

Western Blot

NSCs were lysed in RIPA buffer containing protease inhibitors. Protein amount was determined with a BC assay (Uptima) and equal amounts of proteins were loaded on SDS-PAGE which were then transferred to PVDF membrane (BioRad) by electropherosis. The membrane was then incubated with rabbit anti-SUN1 (1:500) and mouse anti-β-actin (1:5000). HRP-conjugated secondary antibodies (Jackson immunoResearch) were used. The signal was revealed by enhanced chemiluminescence substrate (ThermoScientific).

Retrovirus transduction

90,000 NSCs were first seeded in 12 well plates that had been coated with Poly-L-ornithine (Sigma Aldrich) and Laminin (Sigma Aldrich). Next morning, the media in the wells was changed. Six hours later, 1μl of the retrovirus was added in 500μl of media. The NSCs were then cultured with the virus for one night before the wells were washed with PBS (Thermo Fisher Scientific) and fresh media was added. All experiments were performed at least 5 days post retrovirus transduction, by which time the media had been changed at least 3 times.

Image acquisition and analyses

Zeiss LSM800 and Leica SP8 were used to acquire the images. Overviews of DG were acquired using the tiling function of the Blue Zen (Zeiss) software with a 20X objective and a digital zoom of 0.5X. For DG overviews, tiles were stitched together using Zen Blue. ImageJ/Fiji was used to quantify all the images. The images were blinded before the counting/analysis was performed.

Cell sorting for bulk RNA sequencing

For each replicate, 100 live (propidium iodide$^-$) cells were sorted into one well of a 384 well plate containing lysis buffer using FACSAria III sorter (BD Biosciences). 4 independent biological replicates were sorted for each condition (young NSCs, old NSCs, IRES-GFP old NSCs, LB1 OE IRES-CFP old NSCs). The sorted plate was stored at −80°C until library preparation.

RNA library preparation and sequencing

Library preparation was performed using a mosquito robot HV genomics (TTP Labtech Ltd, UK) following the Smart-seq2 protocol (Jaeger et al., 2020). Briefly, the 384 well plate containing 100 sorted cells per well in lysis buffer was thawed and reverse transcription with Superscript II (Life Technologies) and PCR using KAPA Hifi HotStart ReadyMix (Kapa) were performed with the following biotinylated primers (QIAGEN): Oligodt (AA GCA GTG GTA TCA ACG CAG AGT ACT TTT TTT TTT TTT TTT TTT TTT TTT TTT TTV N), TSO (AAG CAG TGG TAT CAA CGC AGA GTA CATr GrG+G) and ISPCR primers (AA GCA GTG GTA TCA ACG CAG AGT). Following RT-PCR, clean up with Agencourt AMPure XP beads (Beckman Coulter) was carried out and sample concentrations were measured using Bioanalyzer (Agilent Technologies) and normalized at a concentration of 0.3 ng/μl. The Nextera XT DNA library prep kit (Illumina) was used for subsequent sample preparation. Samples were subjected to a tagmentation reaction, indexing, and PCR amplified. Libraries were then mixed in 16-sample pool and purified with Agencourt AMPure XP beads. Ready DNA libraries were quality controlled using D1000 Screen Tape Assay (Agilent Technologies). Samples were sequenced at the Functional Genomics Center Zurich on Illumina NovaSeq 6000 with single-end 150bp reads.

Please cite this article in press as: bin Imtiaz et al., Declining lamin B1 expression mediates age-dependent decreases of hippocampal stem cell activity, Cell Stem Cell (2021), https://doi.org/10.1016/j.stem.2021.01.015

CellPress

QUANTIFICATION AND STATISTICAL ANALYSIS

Statistical Tests

Prism was used to perform all the statistical tests. In all the graphs, mean ± standard error of mean is shown unless otherwise stated. The tests performed are indicated in figure legends. For p values, the following outline was used: ns $p > 0.05$, *$p < 0.05$, **$p < 0.01$, ***$p < 0.001$

RNA-seq analysis

Samples were analyzed using the sushi analysis pipeline from the Functional Genomics Center Zurich (https://fgcz-sushi.uzh.ch/users/sign_in). Reads were adaptor removed and trimmed using cutadapt v2.10 and sickle v1.33 with default parameters. Reads were mapped against the mouse reference genome GRCm38.p6 using STAR v2.7.6a (Dobin et al., 2013). The gene count matrice was quantified at the exon level ignoring multimappers using featureCounts from subread v1.6.3. (Liao et al., 2013). Cells were quality checked using CountQC. Seurat v3.0 (Stuart et al., 2019) was used to normalize read counts and dimensionality reduce the data (Principal Component Analysis). Differential gene expression analysis based on the negative binomial distribution (FDR < 0.05) was performed using DESeq2 v1.30.0 (Love et al., 2014). Data analysis was carried out in R version 4.0.3.